# FRACTURE DENSITY OF UNITS IN THE BRUSHY CANYON FORMATION, WHITEHORSE GROUP AND WINCHELL FORMATION OF THE PERMIAN BASIN.

by

SKYLER SMITH

Presented to the Faculty of the Graduate School of

The University of Texas at Arlington in Fulfillment of the Requirements

for the Degree of

MASTERS OF SCIENCE IN GEOLOGY

THE UNIVERSITY OF TEXAS AT ARLINGTON

AUGUST 2013

ACKNOWLEDGEMENTS

I would like to give my gratitude to the people who have made it possible to reach this point in my academic career including the people at Texas Tech University, Lubbock Texas, at the University of Texas at Arlington, Arlington Texas. In addition I would like to give thanks to my friends and family that have helped me along the way.

I would like to acknowledge the support of my advisor Dr. John Wickham for his advice and guidance through my studies. His support with the initial inception of this project in addition with support throughout the process of this research made this thesis possible. I would like to thank Dr. Xinbao Yu in the Geomechanics Lab for his help with acquiring acoustic velocity information that was invaluable to the results my work.

I would also like to express my appreciation to those who helped throughout the process of acquiring field samples to reading my thesis and giving me their feedback. Mainly I would like to thank my wife Melissa. I would like to thank you for going out into the field with me and being my assistant on all my measurements and pictures. I also want to thank you for pushing me to sit down and work on my thesis, without your love and caring support I do not know how I would have finished my work. Next I would like to thank my mother and father for not only their support in my educational pursuits, reading my thesis and providing me with their suggestions to improve my work, but providing me with the tools I have needed to succeed in life. I want to thank my sister, Brittany for the mental support she has provided me through the years.

August 22, 2013

ABSTRACT

FRACTURE DENSITY OF UNITS IN THE BRUSHY CANYON FORMATION, WHITEHORSE GROUP AND WINCHELL FORMATION OF THE PERMIAN BASIN.

Skyler Smith, M.S.

The University of Texas at Arlington, 2013

Supervising Professor: Dr. John Wickham

This study tests the theoretical equation $\frac{F_d U_a}{\mu} = A\frac{v}{1-2v} + B$, where $F_d$ equals the fracture density present in a geologic unit under constant strain conditions. The material properties in the equation were measured using acoustic velocities and density from samples taken from outcrops. Fracture density was measured from those same outcrop layers. If the equation is valid the measured data should plot as a straight line. The validity of the equation can be estimated using the correlation coefficient of the straight line graph. Fracture density measurements were made within the Permian age Brushy Canyon formation, Whitehorse Group and Winchell Formation of the West Texas Permian Basin. Material properties were obtained from P and S wave velocity measurements made by the Geomechanics Lab at UTA from samples collected from the Permian units mentioned above. Density was also measured from samples taken from the Brushy Canyon Formation, Whitehorse Group and Winchell Formation. Supplemental data for the observed formations were obtained from Wickham (1985) to support and expand the data set collected for this study. The results from the Whitehorse group have a correlation coefficient ≥ .90 indicating that the equation above is valid for those particular outcrops, and may be a good predictor of brittleness. I was unable to get more than three data samples for the other units, so the high correlations may be unreliable. Using the

evaluation criteria in this study the fracture density of a unit has an exponential increase as the unit experienced increasing uniaxial extension. In addition, some units have significantly greater fracture density at a particular strain than others, identifying those layers that are more brittle.

TABLE OF CONTENTS

LIST OF ILLUSTRATIONS

Figure Page

LIST OF TABLES

Table Page

# CHAPTER 1

# INTRODUCTION

Theoretically there is a relationship between the strain energy and fracture density of stratigraphic layers but there has been minimal research to prove the validity of this relationship. There have been many studies on fracture density and fracture spacing over the years. (Narr and Lerche, 1984; Watts, 1983; Willemse et al., 1997; Julander et al., 1999; Tapp et al., 1999; Maulden, Dunne and Rohrbaught, 2001; Di Naccio et al., 2005; Ortega, Marrett and Laubach, 2006; Lorenz Cooper and Olsson, 2006; Mclennan et al., 2009; Zahm and Hennings, 2009; Barthelemy, Guiton and Daniel, 2009). Recently surface fractures have been characterized using seismic properties such as P-wave velocities (Karaman et al., 1997), and shear-wave splitting (Lou and Rial, 1997). Other factures that have recently been used in the measurement of fractures are frequency dependent anisotropy (Maultzsch et al., 2003), and Azimuthal AVO analysis (Xu and Tsvankin, 2007). Additional information about seismic velocities has been obtained from well monitoring. This method has allowed for the observation of deformation associated with fracture or fracture reactivation associated with stress changes or strains in the overburden in fields in real time (Maxwell and Urbancic, 2005). Other studies have focused on how fracture propagation is related to how brittle or ductile a unit is and how this is related to fracture length (Slatt and Abouslieman, 2011).

Research has shown that there are many factors that can affect fracture density within a stratigraphic unit. One factor is layer curvature (Murray, 1968; Stearns and Friedman, 1972; Schultz-Eia and Yeh,1992). Another is strain magnitude which can be derived from cross section restorations (Hennings, Olson and Thompson, 2000). Elastic stress (Bourne and Willemse, 2001), layer thickness and stress shadows (Ladeira and Price, 1981; Huang and Angelier, 1989; Pollard and Segal, 1987), porosity (Lezin et al., 2009), Young's Modulus (Palchik and Hatzor, 2002), and rock strength (Corbett et al., 1987) are additional factors that can influence fracture density.

In the study of fracture density three different approaches have been used: linear regression, Bayesain statistics and probabilistic logic. A study conducted by Lezine and others (2009) used the regression approach. In their study they identified 8 factors that affected fracture density. These factors include: Layer thickness, $CaCO_3$ content, % carbonate grains, % non-carbonate grains,

sparite/micrite ratio, porosity, sonic velocity, and Young's modulus. The Bayesian method was tested by Mclennan et al., (2009) to provide "a quantitative model for the integration of multiple attributes representing the variety of fracture formation mechanisms in play for a particular reservoir…The resulting models of fracture geometry better represent complex fracture heterogeneity and reduce prediction uncertainty" (p. 1586). Their study found "the model of fracture intensity is more geologically realistic than if we were to have not used any attributes or if we were to have selected and used just one of the attributes" (p. 1594). The probabilistic logic model was used by Ja'fari et al., (2012) to test the idea that fracture density can affect the response of conventional well logs. In this study the author used sonic, neutron porosity, deep resistivity, and bulk density for their analysis. The authors found the best correlations occurred between fracture density per meter and the bulk density and the sonic logs.

## 1.1 Theoretical Foundation

Table 1. Symbols used in paper.

| Symbol | Meaning | Units |
|---|---|---|
| U | Energy | N*m |
| $U_v$ | Strain energy in volume v | $N*m/m^3$ |
| V | Volume | $m^3$ |
| A | Area | $m^2$ |
| G | Energy release rate | $N*m/m^2$ |
| ε | Stress | MPa |
| E | Strain | MPa |
| $F_d$ | Fracture Density | $F_d/M^{-1}$ |
| $U_a$ | Energy per fracture area created | |
| μ | Elastic Shear Modulus | GPa |
| $v$ | Poisson's Ratio | |
| E | Young's Modulus | GPa |
| ρ | Mass Density | $g/cm^3$ |
| $V_p$ | Compressional Wave Velocity | Km/s |
| $V_s$ | Shear Wave Velocity | Km/s |
| $I_1$ | First Strain Invariant | |
| $I_2$ | Second Strain Invariant | |
| $K_{IC}$. $K_{IIC}$, $K_{IIIC}$ | Fracture Toughness for mode I, II, and III | MPa√m |

Fracture density is defined as fracture surface area/volume. (See Table 1 for symbols used in this section). In the hydraulic fracturing process used in the petroleum industry, the greater the fracture density, the greater the hydrocarbon recovery. Therefore it is important to know in advance whether the induced fracture density in a reservoir is likely to be high or low and how the hydraulic fracture design can be improved. The theoretical foundation established by Wickham et al., (2013) outlined the process of obtaining fracture density from the material properties of rock units and some of the language used by Wickham et al., (2013) is repeated here.

Strain-energy density is the area under a stress-strain curve:

$$U_V = \int_{\varepsilon_0}^{\varepsilon_1} \sigma_x d\varepsilon_x \qquad \text{(Eq. 1)}$$

$U_v$ it the total elastic strain energy in the system at the point of failure. In Eq. 1 $\varepsilon_1$ is equal to the strain upon failure, $\sigma_x$ is the stress component and $\varepsilon_x$ is the strain component in a solid (Sih, 1985). A.A. Griffith (1921) developed a fracture criterion based on strain energy. More recently, G.C. Sih (1985) has presented a

more comprehensive theory. He summarizes it as "The strain energy density theory in its most basic form can be formulated from the basic hypothesis that the surface and volume energy density of each material element are related by the rate of change of volume with surface" (Sih, 1985 p.167).

Symbolically,

$$\left(\frac{dA}{dV}\right)_i \left(\frac{dU}{dA}\right)_i = \left(\frac{dU}{dV}\right) \qquad \text{(Eq. 2)}$$

Where "A" is fracture surface area, V equals volume, and U is the strain energy. This theory is written as a differential equation but for the purpose of this study the integrated form that places the theory over a volume element is more useful:

$$\frac{AU_a}{V} = \frac{U_v}{V}$$

Simplifying the variables gives:

$$(F_d)(U_a) = U_v \qquad \text{(Eq. 3)}$$

$F_d$ = Fracture density (fracture surface area in the volume of interest); $U_a$ = energy per fracture area created, considered a material property; $U_v$ = elastic strain energy density in the volume of interest. $U_a$ in this formula is not just fracture surface energy, but all the energy that goes into producing new surface area associated with a fracture which includes: new fracture surface energy, energy dissipated as heat, acoustic emissions and other crack growth in the process zone. In addition $U_a$ takes into account the energy associated with damage and plastic deformation emphasized by Busetti et al., (2012). $U_v$ is the elastic strain energy associated with volume change and, for this study, the simplifying assumption that all the energy for $U_a$ comes from $U_v$. Below the elastic yield point $U_v$ might be associated with closing cracks and a reduction of fracture density. Above the yield point $U_v$ can be associated with increasing volume, fracture density and plastic deformation. Above the yield point, it is assumed that the matrix material away from the fracture and damage zones continues to behave elastically building elastic strain energy; however, some of that elastic energy, $U_v$, is converted into fracture energy. In this approach, whether the material yields in tension or compression should not have an effect on the results.

The results of this theory is that fracture density measured over some volume of rock is a function of the strain energy in that same volume of rock at the same time the fractures formed. Strain energy density is expressed in a generalized form as:

$$U_V = \frac{1}{2}\left(\sigma_{xx}\epsilon_{xx} + \sigma_{yy}\epsilon_{yy} + \sigma_{zz}\epsilon_{zz}\right) + \left(\sigma_{xy}\epsilon_{xy} + \sigma_{yz}\epsilon_{yz} + \sigma_{xz}\epsilon_{xz}\right) \qquad \text{(Eq. 4)}$$

It is assumed that up to the yield point all the strain experienced is elastic and above the yield point and the matrix material away from the damage zones is deforming elastically as well. Some of the elastic strain energy present within the matrix is now used to create more fracture surfaces instead of elastic distortion.

With the assumption of elasticity, strain energy density in a rock volume of constant elastic properties is:

$$U_V = \frac{v\mu}{1-2v}\left(\epsilon_{xx} + \epsilon_{yy} + \epsilon_{zz}\right)^2 + \mu\left(\epsilon_{xx}^2 + \epsilon_{yy}^2 + \epsilon_{zz}^2\right)^2 + 2\mu\left(\epsilon_{xy}^2 + \epsilon_{yz}^2 + \epsilon_{xz}^2\right)^2 \qquad \text{(Eq. 5)}$$

v = Poisson's ratio and $\mu$ = shear modulus. $U_v$ is the total elastic strain energy. Assuming strain is constant within the observed rock units, Eq. 5 becomes:

$$U_V = \mu\left(A\frac{v}{1-2v} + B\right) \qquad \text{(Eq. 6)}$$

Where A and B are constants related to strain state and can be defined as:

$$A = I_1^2$$

and:

$$B = I_1^2 - 2I_2$$

Where $I_1$ = first strain invariant and $I_2$ = second strain invariant. When these identities are applied, Eq. 3 becomes:

$$F_d = \frac{\mu}{U_a}\left(A\frac{v}{1-2v} + B\right) \qquad \text{(Eq. 7a)}$$

The goal of this thesis is to test the validity of Eq. 7a under constant strain conditions. Rewriting, Eq. 7a becomes:

$$\frac{F_d U_a}{\mu} = A\frac{v}{1-2v} + B \qquad \text{(Eq. 7b)}$$

This equation shows that fracture density and material properties should plot as a straight line at the strain state represented by A and B.

The elastic properties of rock samples collected from the Brushy Canyon, Whitehorse group and Winchell Formation can be estimated by the acoustic wave properties and density values acquired by the Geomechanics Lab at The University of Texas at Arlington. To calculate the shear modulus, S wave velocity can be used, as shown in Eq. 8; to obtain Poisson's ratio both the P and S wave acoustic properties are used as shown in Eq. 9.

$$\mu = V_s^2 \rho \qquad \text{(Eq. 8)}$$

$$v = \frac{\frac{1}{2}\left(\frac{V_p}{V_s}\right)^2 - 1}{\frac{V_p}{V_s} - 1} \qquad \text{(Eq. 9)}$$

$V_p$ = compressional wave velocity; $V_s$ = shear wave velocity; and ρ = density (Sheriff, R. E., 1991).

Equation 7b can be written as a formula using acoustic velocity data. When the values for the elastic shear modulus, μ, and poisons ratio, $v$, are substituted with Eq. 8 and 9 respectively, Eq. 7a becomes:

$$F_d U_a = V_s^2 \rho \left( A \frac{\frac{\frac{1}{2}\left(\frac{V_p}{V_s}\right)^2 - 1}{\frac{V_p}{V_s} - 1}}{1 - 2\left(\frac{\frac{1}{2}\left(\frac{V_p}{V_s}\right)^2 - 1}{\frac{V_p}{V_s} - 1}\right)} + B \right) \qquad \text{(Eq. 10)}$$

The fracture surface energy in Eq.10, $U_a$, is related to the critical energy release rate $G_c$. For brittle elastic materials Eq. 11 can be derived (Backers T. 2005):

$$G_c = 2U_a \qquad \text{(Eq. 11)}$$

Rock fractures can be subdivided into three types; mode I, II, and III (Irwin, 1956). The differences between the three modes of fracture are distinguished by fracture surface displacement (Figure 1) (Lawn, 1993). The equivalence of the energy release rate and the critical stress intensity factor ($K_c$) has been shown by Irwin, 1956. As the principle of superposition applies to the three crack modes, energy release rates can be obtained as:

$$G_c = \frac{K_{IC}^2}{E} + \frac{K_{IIC}^2}{E} + \frac{K_{IIIC}^2(1+v)}{E} \qquad \text{(Eq. 12)}$$

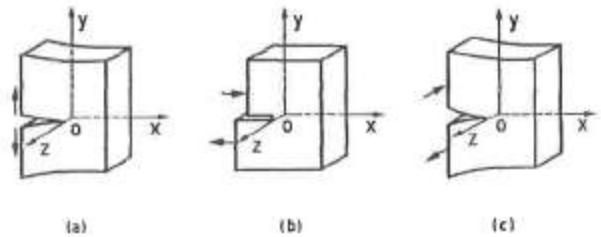


Figure 1. The three basic modes of fracture, (a) Opening mode I, (b) Sliding mode II, and (c) Tearing (or antiplane) mode III; (Gdoutos, 2005).

Because joints were measured in the field it is assumed that mode I fractures are dominant. In mode I, or opening (tensile) mode, the fracture tip is subjected to displacement perpendicular to the crack plane and experiences no evidence of shear displacement (Backers, 2004). The assumption about the fracture mode measuredin the outcrop allows Eq. 12 to be simplified as (Atkinson 1987):

$$G_c = \frac{K_{IC}^2}{E} \qquad \text{(Eq. 13)}$$

Where $K_{IC}$= Fracture toughness; and E = Young's Modulus. Fracture toughness is defined as the point at which fracture extension will occur when the stress intensity factor reaches a critical value (Backers, 2004). This results in $U_a$ being expressed as:

$$U_a = \frac{\left(\frac{K_{IC}^2}{E}\right)}{2} \qquad \text{(Eq. 14)}$$

Ua, is related to the critical energy release rate, $G_c$, as indicated in Eq. 11. To calculate $G_{c,}$ the fracture toughness factor of a rock unit must be known. The stress intensity factor of a unit can found though laboratory measurements of a rocks fracture toughness, $K_{IC}$. To measure fracture toughness a variety of methods can be used including: the Semicircular Core in Three Point Bending test (Chong & Kuruppu, 1984), the chevron-notched SCB test (Kuruppu, 1997), the Brazilian Disc test (Guo et al., 1993), the Radial Cracked Ring test (Shiryaev and Kotkis, 1982), the Modified Ring test (Thiercelin and Roegiers, 1986), and the Double Torsion test (Evans, 1972). The International Society for Rock Mechanics (ISRM) recommends the three methods illustrated in Figure 2, which includes the Cheveron Bend, the Short Rod method and the Cracked Cheveron Notched Brazilian Disk Method (Ouchterlony,

1988; Fowell, 1995). All of the above methods measure the amount of force that is required to initiate fracture within a sample where $K_{IC}$ is the measure of resistance to the extension of fracture that the rock experiences (Zhixi et al. 1997).

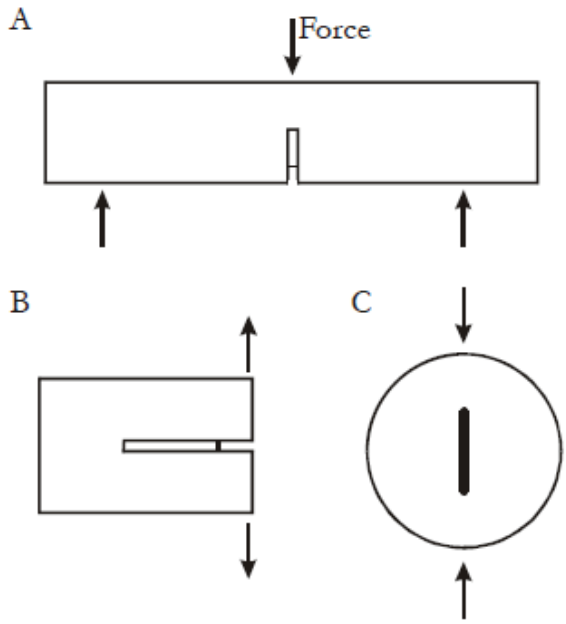


Figure 2. ISRM Suggested Methods for determination of Mode I fracture toughness. A: Chevron Bend (CB-) method; B: Short Rod (SR) method (both Ouchterlony, 1988) and C: CCNBD (Cracked Chevron Notched Bra-zilian Disc) method (Fowell, 1995).

Fracture toughness can be expressed in terms of acoustic velocity as defined by Whittaker et al., (1992) and Huang and Wang (1985). They found there is a statistical correlation between $K_{IC}$ and different physical properties through a variety of equations. To test their theory the fracture toughness for all types of sedimentary rock, excluding conglomerates was measured and then compared to the calculated predictive results. (Table 2 and 3):

Table 2. Variables outlined by Whittaker et al 1992.

| Symbols used by Whittaker et al 1992 | |
|---|---|
| Symbol | Meaning |
| $K_{IC}$ | Critical Stress intensity factor |
| $\sigma_C$ | Uniaxial Compressive Strength |
| $\sigma_t$ | Tensile Strength |
| $H_T$ | Total Hardness: $H_T = Hss\sqrt{H_A}$, where $H_A$ is the modified Taber abrasion hardness. |
| Hss | Shore scleroscope hardness |
| I | Point Load Strength |
| $\sigma_{fr}$ | Flexure Ridgity |
| E | Young's modulus |
| $v_p$ | P wave velocity |

Table 3. Equations outlined by Whittaker Et al 1992.

| Equation | R |
|---|---|
| $K_{IC}=0.708+.006\sigma_C$ | 0.72 |
| $K_{IC}=0.271+.107\sigma_t$ | 0.83 |
| $K_{IC}=.72+.02xH_T$ | 0.73 |
| $K_{IC}=1.331+0.074 X I$ | 0.49 |
| $K_{IC}=0.042+0.039\sigma_{fr}$ | 0.85 |
| $K_{IC}=0.313+0.027E$ | 0.86 |
| $K_{IC}=-1.68+0.65v_p$ | 0.9 |

$$K_{IC} = -1.68 + 0.65(V_p) \quad \text{(Eq. 15)}$$

The relationship between fracture toughness, rock toughness and acoustic properties (Eq. 15) was shown to contain the highest correlation between the calculated and measured $K_{IC}$ values presented by Whittaker et al., 1992.

The work conducted by Whittaker et al., 1992 has shown this Eq. 15 has a correlation coefficient of 0.90 when compared to laboratory measured results and can be used to predict fracture toughness values using P wave velocities (Figure 3). The ability to predict fracture toughness for the desired rock unit compared to using established values found in literature for one rock type is desirable. Rock toughness can very between like rock types, such as limestone, because variability in grain size and porosity in a can vary from one unit to the next resulting in changes in fracture toughness.

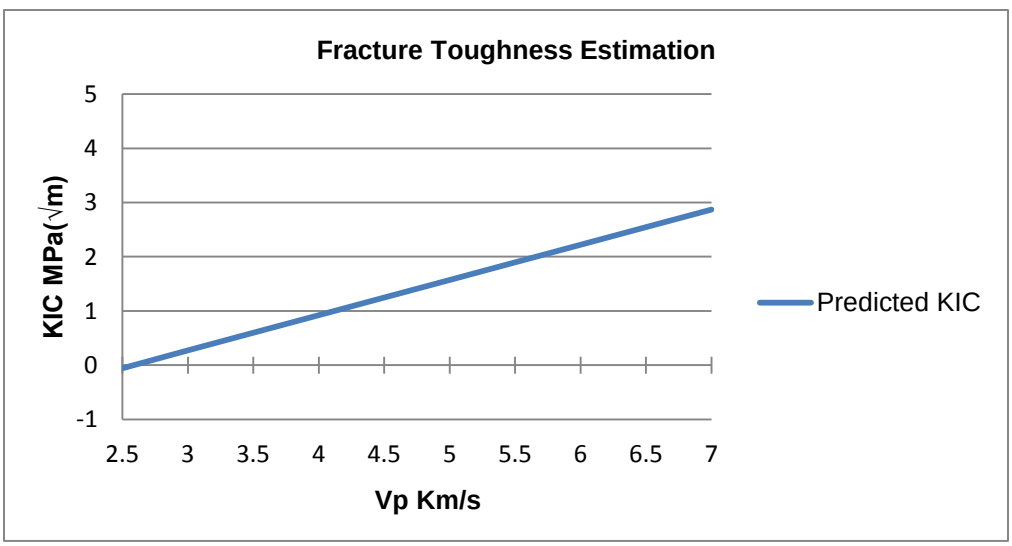


Figure 3. Fracture Toughness estimation from Eq. 15.

Eq. 15 can be used to calculate $K_{IC}$ using easily obtainable rock properties. In addition, this equation is the least expensive and time consuming method of obtaining reasonable $K_{IC}$ values,

When Eq. 14 and 15 are applied to Eq. 10, it becomes:

$$F_d\left(\frac{\left(\frac{\left(-1.68+0.65(V_p)\right)^2}{E}\right)}{2}\right) = V_s^2\rho\left(A\frac{\frac{\frac{1}{2}\left(\frac{V_p}{V_s}\right)^2-1}{\frac{V_p}{V_s}-1}}{1-2\left(\frac{\frac{1}{2}\left(\frac{V_p}{V_s}\right)^2-1}{\frac{V_p}{V_s}-1}\right)}+B\right) \qquad \text{(Eq. 16)}$$

Young's modulus can be expressed in terms of acoustic velocity and density McCann and Entwisle, 1992:

$$E = 2\rho V_s^2(1-v) \qquad \text{(Eq. 17)}$$

Rewritten in terms of acoustic velocity for Poisson's Ratio, Eq. 17 becomes:

$$E = 2\rho V_s^2\left(1-\left(\frac{\frac{1}{2}\left(\frac{V_p}{V_s}\right)^2-1}{\frac{V_p}{V_s}-1}\right)\right) \qquad \text{(Eq. 18)}$$

When applied to Eq. 16:

$$F_d\left(\frac{\left(\frac{\left(-1.68+0.65(V_p)\right)^2}{2\rho V_s^2\left(1-\left(\frac{\frac{1}{2}\left(\frac{V_p}{V_s}\right)^2-1}{\frac{V_p}{V_s}-1}\right)\right)}\right)}{2}\right) = V_s^2\rho\left(A\frac{\frac{\frac{1}{2}\left(\frac{V_p}{V_s}\right)^2-1}{\frac{V_p}{V_s}-1}}{1-2\left(\frac{\frac{1}{2}\left(\frac{V_p}{V_s}\right)^2-1}{\frac{V_p}{V_s}-1}\right)}+B\right) \qquad \text{(Eq. 19)}$$

To calculate the A and B, which will be calculated in this thesis, and to test the assumptions being made, Eq. 7b can be rewritten as:

$$\frac{F_d\left(\frac{\left(\frac{\left(-1.68+0.65(V_p)\right)^2}{2\rho V_S^2\left(1-\left(\frac{\frac{1}{2}\left(\frac{V_p}{V_S}\right)^2-1}{\frac{V_p}{V_S}-1}\right)\right)}\right)}{2}\right)}{V_S^2\rho} = \left(A\frac{\frac{\frac{1}{2}\left(\frac{V_p}{V_S}\right)^2-1}{\frac{V_p}{V_S}-1}}{1-2\left(\frac{\frac{1}{2}\left(\frac{V_p}{V_S}\right)^2-1}{\frac{V_p}{V_S}-1}\right)}+B\right) \qquad \text{(Eq. 20)}$$

$$Fd = \frac{V_S^2\rho}{\left(\frac{\left(\frac{\left(-1.68+0.65(V_p)\right)^2}{2\rho V_S^2\left(1-\left(\frac{\frac{1}{2}\left(\frac{V_p}{V_S}\right)^2-1}{\frac{V_p}{V_S}-1}\right)\right)}\right)}{2}\right)}\left(A\frac{\frac{\frac{1}{2}\left(\frac{V_p}{V_S}\right)^2-1}{\frac{V_p}{V_S}-1}}{1-2\left(\frac{\frac{1}{2}\left(\frac{V_p}{V_S}\right)^2-1}{\frac{V_p}{V_S}-1}\right)}+B\right) \qquad \text{(Eq. 21)}$$

Equation 7b and Eq. 20 are used in this study to verify that Eq. 7a and 21 are valid under constant strain conditions. The graph that is generated by the material properties in Eq. 20 should plot in a straight line with the slope of the line being related to the first strain invariant, A and both the first and second invariant being related to the intercept, B. If the linear relationship is shown to have a correlation of ≥ 0.90, Eq. 7a will be verified.

CHAPTER 2

GEOLOGIC SETTING

For this study, two basins are used to provide a range of geological settings and conditions that can have an effect on fracture development within various stratigraphic units in a single outcrop. The outcrops are located in the Whitehorse Group and The Winchell Formation along the Eastern Shelf of the Midland Basin and in the Brushy Canyon Formation located in the Delaware Basin. Both the Eastern shelf of the Midland Basin and the Delaware Basin are found within the Permian Basin. The Permian Basin is an asymmetrical, foreland basin covering 222,739 km$^2$ located in west Texas and southeastern New Mexico that formed as a flexural response to the vertical loading of the Marathon – Ouachita foldbelt (Yang and Dorobek, 1995). The Permian Basin is bounded by the Matador Arch to the north, the Marathon – Ouachita Fold Belt to the south, the Diablo Platform and Pedernal Uplift to the west and the Eastern Shelf of the Midland Basin. The basin is divided into several distinct uplifts including: the Central Basin Platform and the Ozona Arch, separating the Delaware Basin from the Val Verde Basin to the south and the Midland Basin to the north and east (Ball, 1995) (Figure 4 and 5).

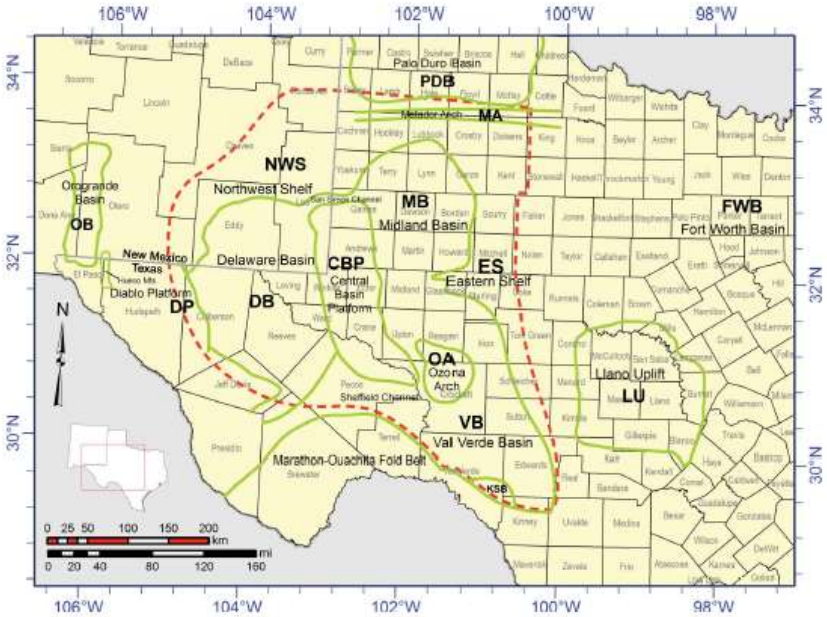


Figure 4. Regional map of the Permian Basin (red). Main physiographic features outlined (green). (Dutton et al., 2005; Wright, 2011).

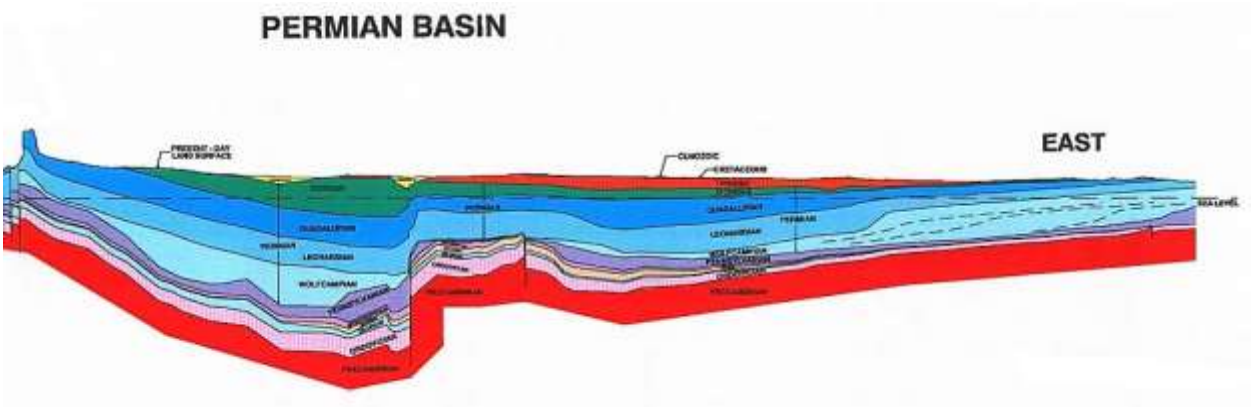


Figure 5. West to East cross section of the Permian Basin. (Lindsay, 2009).

## 2.1 Eastern Shelf of the Midland Basin

The Eastern Shelf of the Midland Basin is a paleo-marine shelf, resembling modern continental shelves, which covers an area of 25,900 $km^2$ and lies upon the older Concho platform to the east of the Midland basin. The shelf consists predominantly of carbonate rock of Permian age that grades to the east into back reef dolomites, anhydrites and red beds that were formed in a variety of sedimentary environments including: deltaic, embayment, open marine shelf and shelf edge banks (Martin et al., 1953; Galloway and Brown, 1973).

### 2.1.1 Whitehorse Group

The Whitehorse Group is a Guadalupian age marine deposit that consists of the Grayburg formation, Queen Formation, Seven Rivers Formation, Yates Sand and the Tansill formation (Page and Adams, 1940). The Grayburg formation is characterized by dolomite and sand beds together with minor amounts of shale and bentonite. The Queen formation consists of fined grained sandstones with interbedded anhydrites. Above the Queen formation is the Seven Rivers formation, which is predominantly salt with anhydrite and minor amounts of fine grained sand and dolomite. The Yates sand is uniform, fine grained quartz sand with interbedded shale and anhydrite stringers. The Tansill formation contains anhydrite and consists of minor beds of salt, sandstone and shale (Page and Adams, 1940).

### 2.1.2 Winchell Formation

The Winchell formation is a Pennsylvanian age unit of the Canyon group in the Eastern shelf and is divided into two limestone sequences separated by a thick shale interval with a total thickness of about 100 ft. The lower Winchell contains three or more limestone beds bounded by shale and sandstone, and the upper Winchell contains two limestone units bounded by shale and sandstone (Myers, 1955).

## 2.2 Delaware Basin

The Delaware Basin is a major Depression in the westernmost portion of the Permian Basin province located in west Texas and southeast New Mexico (Hills and Galley, 1988; Luo 1992; Luo et al., 1994). The basin has an asymmetric shape and is bounded on three sides by major uplifts: the Marathon fold and thrust belt to the south, the Central Basin platform to the east and the Diablo platform to the west (Montgomery et al., 1999).

The geologic history of the Delaware basin consists of four periods of sedimentation and tectonic activity. During the first period, ranging from Ordovician to Devonian the area consisted of a broad carbonate platform (Hills and Galley, 1998) without significant faulting (Luo et al., 1994).

Tectonic collision between the South American Plate and the North American Craton occurred in the second period during the Mississippian. This period of collision caused vertical movement of fault zones along the eastern portion of the basin with significant strike-slip offset resulting in uplift of the Central Basin Platform (Hills, 1970). The sedimentary environment during this time changed to deep water (Luo et al., 1994).

The third period occurred during Pennsylvanian through Permian time. During the Pennsylvanian the Delaware Basin became a sediment starved basin due to the formation of carbonate banks that developed in the northeast (Adams et al., 1951; Hills, 1984). In the Permian, intervals of tectonic quiescence lead to the deposition of thin limestone intervals. In the deeper parts of the basin, saline density currents deposited thick sandstone layers followed by periods of less dense interflows of silt

(Harms and Williamson, 1988). The Delaware Mountain Group, consisting of the Brushy Canyon formation, Cherry Canyon formation and the Bell Canyon formation, was deposited during this period.

The fourth division of the Delaware Basin history occurred during Mesozoic through Cenozoic time When the basin experienced sea level rise and fall; and shore lines regressed and transgressed (Hills, 1984) resulting in subaerial erosion and evaporate dissolution of the upper Permian beds (Maley and Huffington, 1953)

### 2.2.1 Brushy Canyon Formation

The Brushy Canyon Formation is one of the units used for fracture density measurements in this study. The Brushy Canyon formation is a high energy turbidity current deposit represented by sandstone interbedded with fine grained sand and silts that was deposited during the Guadeloupian period (Harms and Charles, 1998). Texturally, the Brushy Canyon formation consists of angular to sub angular, moderate to well sorted, fine to very fine grained sandstones. The sandstones have a composition containing 60 – 80 % quartz, 20 – 30 % feldspar, 5 – 12% fragments and 2 – 12% clays. (Montgomery et al., 1999)

# CHAPTER 3

# METHODS

Fracture density measurements were taken from uniformly dipping sedimentary rocks within the Brushy Canyon Formation of the Delaware Basin near the Guadalupe Mountains, Texas; the Whitehorse Group of the Permian Basin, near San Angelo, Texas; and The Winchell Formation of the Permian Basin near Brownwood, Texas. Fracture density measurements were made of different lithological units within each outcrop. The units of interest were generally characterized by brittle sedimentary deposits bounded by more ductile shale units. Different sedimentary compositions were measured at the same outcrop to insure fracture density and the material properties of one lithological unit is different from those measured in the other layers. It is assumed that the different measured layers within the same outcrop were subjected to the same amount of strain and will plot along a straight line when the data is applied to Eq. 20.

Samples from the layers where the fracture density was measured were collected to measure the elastic constants by the UTA Engineering Geomechanics Lab

## 3.1 Field Measurements

Various methods were used to measure fracture density in the outcrops. In this study, the method described by Chiles et al., (2008) was used. This method involves measuring various properties of the fracture and the layer containing it: 1) the distance to fractures along a scanline on an exposed area of a layer; 2) the length of each fracture that crosses the scanline; 3) the fracture orientation; 4) the thickness of the layer containing the fracture; 5) the orientation of the layer; 6) the orientation of the area that contains the scanline; 7) the orientation of the scanline; and 8) what, if any, curvature of the bed is present. This information can be used to calculate an unbiased estimate of fracture density (Chiles et al., 2008).

Some problems were encountered in the field when measuring fracture density. The best outcrops that provide access to the units to be measured are road cuts. However, road cuts are commonly created from blasting, which can result in the development of artificial fractures within the outcrop. For that reason, measurements were confined to regional joint sets. Regional joints are mode I (extensional) fractures usually produced from the release of lithostatic pressure and membrane strain as the rock units were uplifted and overburden eroded. In addition, the strain associated with regional joints is most likely consistent from one stratigraphic layer to the next within a given outcrop. The fractures that are associated with blasting can be distinguished from regional joints easily because the fractures that are formed from blasting tend to be confined to a small volume around the drill hole location, are smaller, irregularly shaped, closely spaced and have a radial orientation in relation to the drill hole.

The size of the measurement area along the bedding layer is dependent of the fracture spacing within the unit. The measurement area needed to be large enough to get a statistical sample of the fractures. Depending on the size of the area, two or more scan lines, parallel and perpendicular to each other, were used to record the number of fractures (Figure 6). Because the outcrop area is a sample of the volume, the fracture spacing on the sample area is biased depending on the angle of the fracture in relation to the outcrop surface. For example, fractures that are nearly parallel to the measurement area are underrepresented in the fracture density results. To correct this bias, the angle between the fracture and the measurement surface must be calculated, using an algorithm similar to Chiles, et al., (2008). This algorithm sets a weighting factor for the fractures based on their orientation relative to the scan line giving more emphasis on the fractures that are less perpendicular to the scanline. This allows for proper representation of fractures that might be under represented due to their angle relative to the surface of the unit.

The first area measured was the Brushy Canyon formation. The outcrop location was chosen from Geology of the Delaware Basin and Field Trip Guidebook (West Texas Geologic Society, 1960). Units were measured along stops 5 and 6 to accurately sample the fracture density of different units in the formation. Measurements along stop 5 were taken in non-deformed sandstone units bounded by shale (Figure 6 and 7).

Figure 6. Scanline measurements along the Brushy Canyon formation.

Samples were collected from the measured sandstone and shale units. The shale unit was poorly lithified, and once removed from the outcrop, samples fell apart. Stop 6 is stratigraphicly lower than the units measured at stop 5; only the sand stone units could be reliably measured. Measurements of the shale units within this outcrop were deemed unreliable due to weathering producing secondary fractures that could not be distinguished from natural fractures. In the field it was not possible to distinguish regional joints from secondary fracturing due to weathering. A sample of the measured sandstone unit was collected to use in laboratory measurements.

Figure 7. Brushy Canyon outcrop, Guadalupe Mountains.

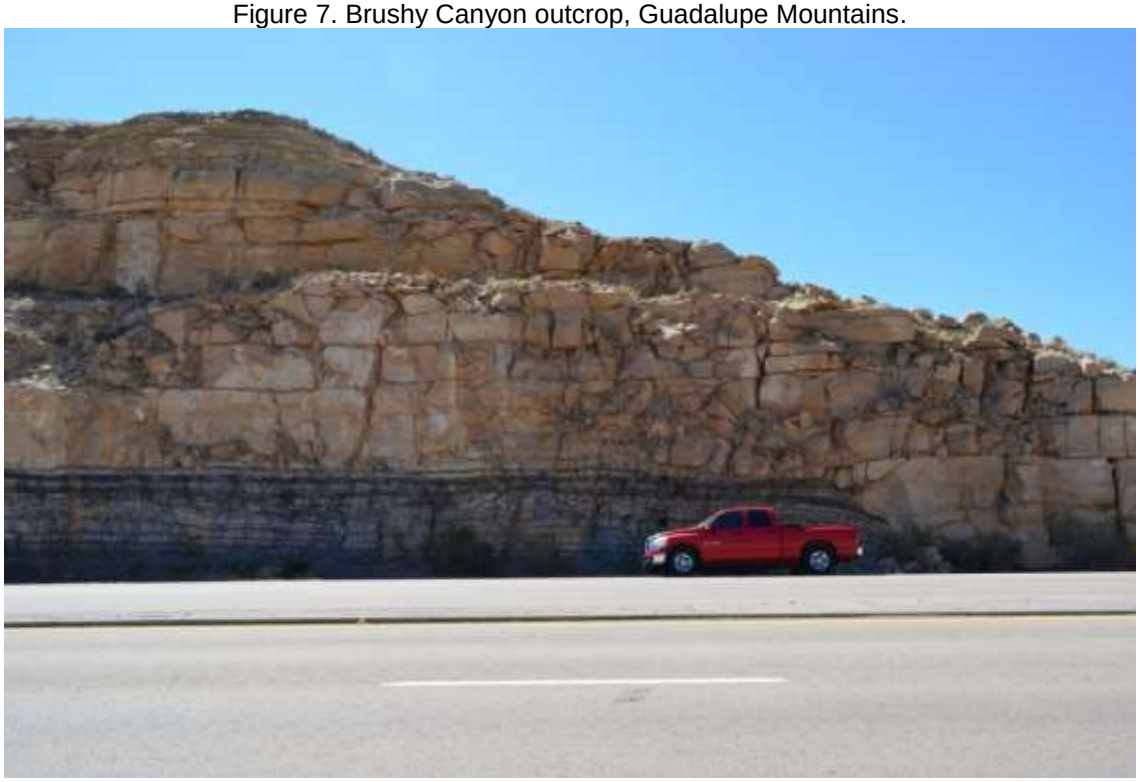

Figure 8. Brushy Canyon outcrop locality 2.

Figure 9. Brushy Canyon Scanline 3.

The second fracture density measurements were acquired within the Winchell Formation (Figure 10). Two units within this formation were measured, the lower limestone unit and the upper shale that separates the upper and lower limestone. Scan line measurements were taken along the exposed face (Figure 11) and along the exposed surface of the limestone (Figure 12). Due to the lower limestone unit's upper surface being exposed, measurements of the fractures were acquired with four scan lines in a grid pattern (Figure 13). The samples collected from this unit were not large enough for reliable laboratory measurements.

Figure 10. Winchell Formation

Figure 11. Lower Winchell limestone.

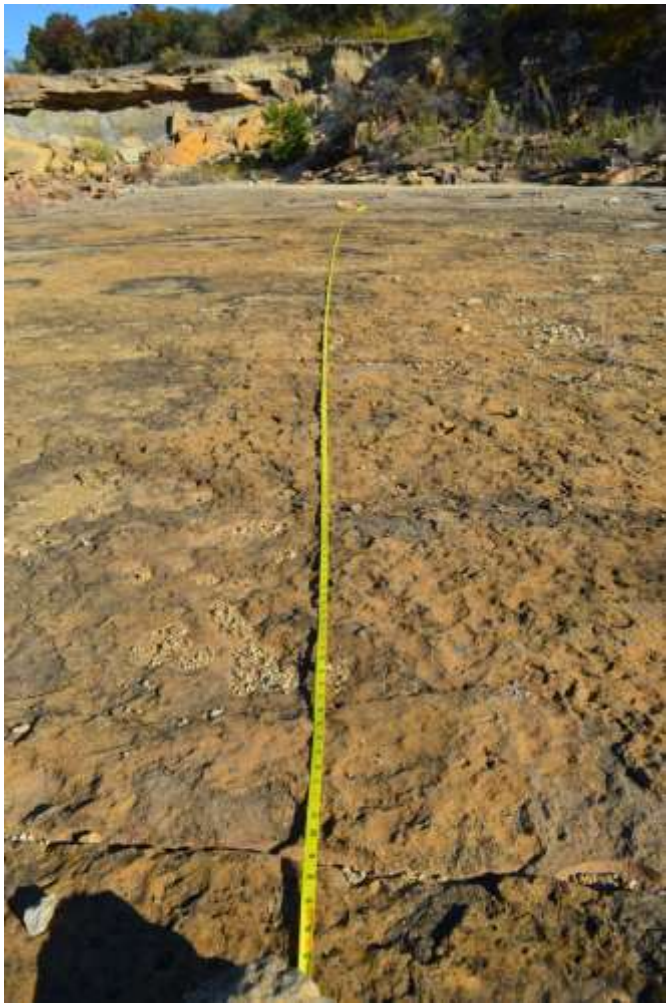

Figure 12. Lower Winchell Limestone surface scanline.

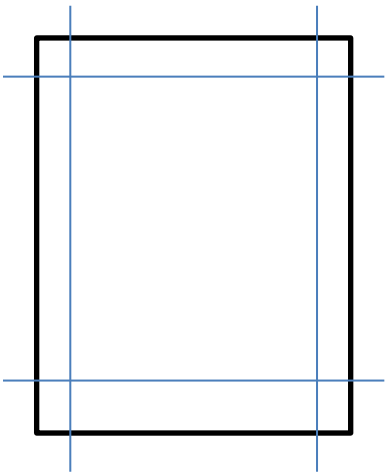

Figure 13. Diagram illustrating scanline measurements taken along the lower Winchell limestone surface.

Measurements were taken of the Whitehorse Group (Figure 14). Due to the best outcrop exposure being present in riverbeds and drainage pathways, finding suitable units was difficult. The scan line method was used; however, the upper sandstone unit had eroded to a curved surface which can alter the spacing of the fractures recorded (Figure 15).

Figure 14. Whitehorse Group Dolomite, scanline 1.

Figure 15. Upper Whitehorse group sandstone

In addition to the field measurements of fracture density, supplemental measurements obtained from Wickham (1985) were used to expand the data set available. These measurements were along the same outcrop locations for the Brushy Canyon formation and the Winchell limestone formation. The measurements conducted along the Whitehorse Group were taken in locations chosen from the SEPM Guidebook #84-23, 1984 Stop 1(Grover, 1984).

## 3.2 Laboratory Measurements

Properties that could not be directly measured in the field including specimen density, elastic properties and fracture surface energy were measured with the help of the engineering Geomechanics Lab at UTA.

### 3.2.1 Acoustic Properties

The acoustic properties to be measured within the collected field samples include the pressure and shear wave, or P and S wave velocities. The P wave velocity measures the amount of time in km/s that the primary wave or pressure wave taken to pass through the sample parallel to the wave direction.

The S wave measures the shear wave travel time, similar to P wave velocity measurements, but the material particles of the S wave vibrate perpendicular to wave propagation. The S wave travels slower through a medium so in acoustic testing the S wave signal will appear last.

To obtain acoustic properties, only samples of a diameter of 6D and a length of 12D minimum (D representing the grain size of the sample) collected from the units in which fracture density was measured were used. To make the samples usable for sonic measurements, they were cut using an automated rock cutter to make two smooth surfaces on which seismic sensors can be attached (Figure 16). The samples were measured by Dr. Yu in the Geomechanics Lab to obtain acoustic velocities. The testing procedure followed the ASTM standard (ASTM 2000). The set up for the ultrasonic velocity test include an ultrasonic pulsar/receiver (Model 5077 PR, Olympus), a PC oscilloscope (PicoScope 5023, pico technology) and ultrasonic transducers (V101 – RB and V150 – RB, Olympus for p – wave and s- wave velocities) The ultrasonic transducers were attached to the smooth rock surface using the Panametrics – NDT SWC couplant to make sure acoustic energy is transmitted between the rock sample and the transducer.


Figure 16. Field samples tested by the Geomechanics Lab. SAUS: Upper sandstone of the White horse group (Rock 1). SALLS: Weathered Dolomite of the Whitehorse Group (Rock 2). BCS2: Lower sandstone of the Brushy Canyon Formation (Rock 3).

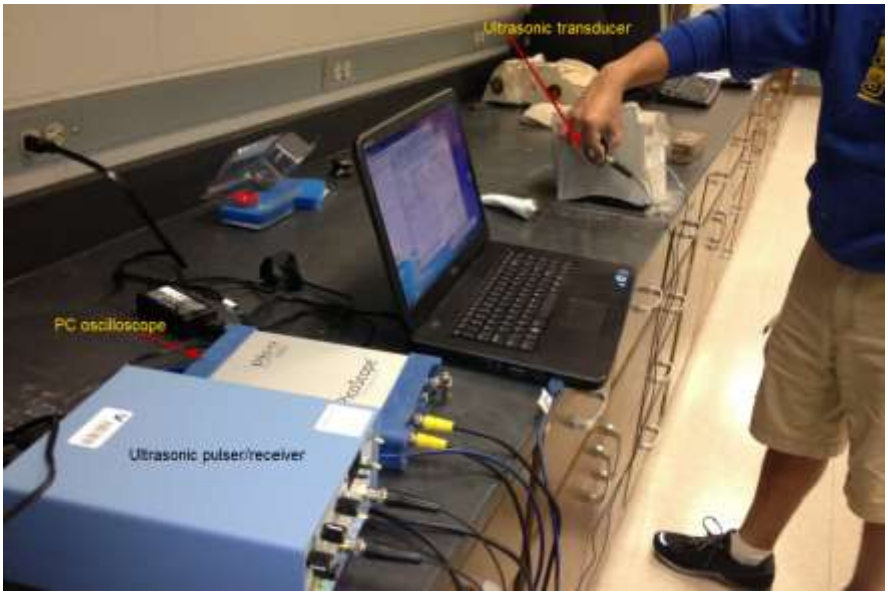


Figure 17. Test of acoustic velocities in the Geomechanics lab at UTA

To transmit and receive the ultrasonic signal a transducer was attached to each side of the rock sample. To acquire the wave velocities from the acoustic signals, the peak-to-peak method was used (Figure 18 - 23). The velocity that is recorded is represented by the amount of time that the signal, the first peak (red arrow), to the first peak of the signal reaching the transducer on the opposite side of the sample, (Green Arrow) (Figure18).

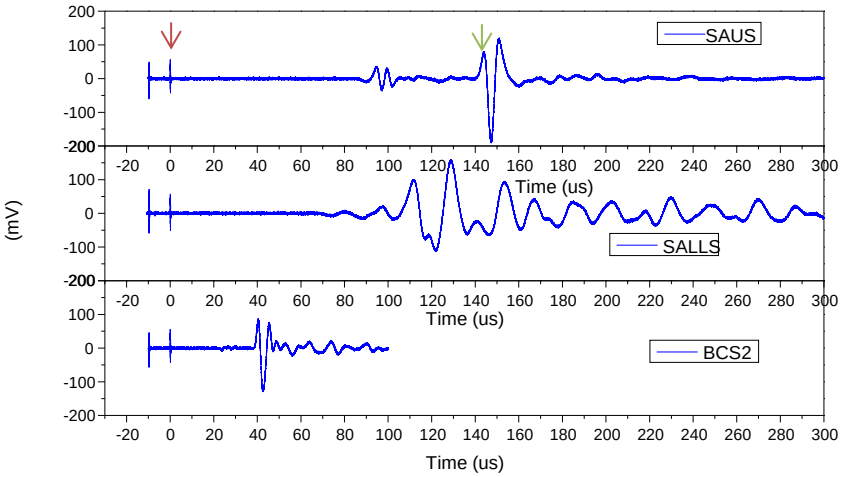


Figure 18. S-wave signal for sample SAUS and SALLS of the Whitehorse formation and BCS2 of the Brushy Canyon Formation

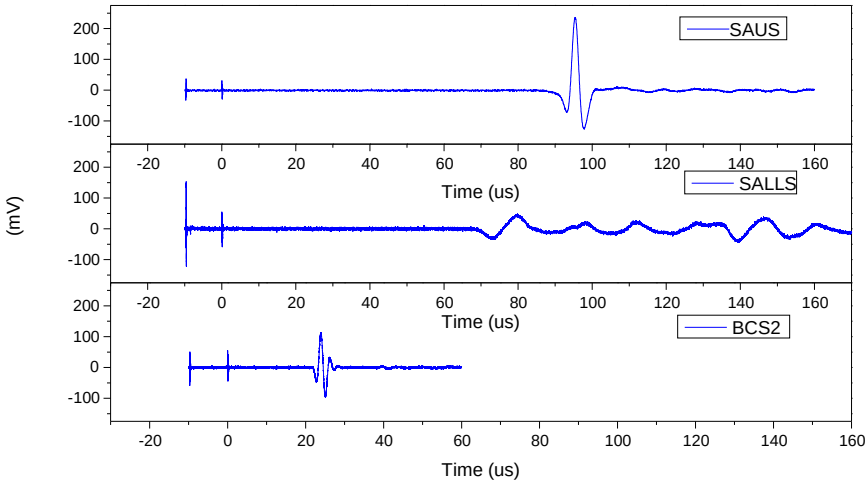


Figure 19. P-wave signal for sample SAUS and SALLS of the Whitehorse formation and BCS2 of the Brushy Canyon Formation

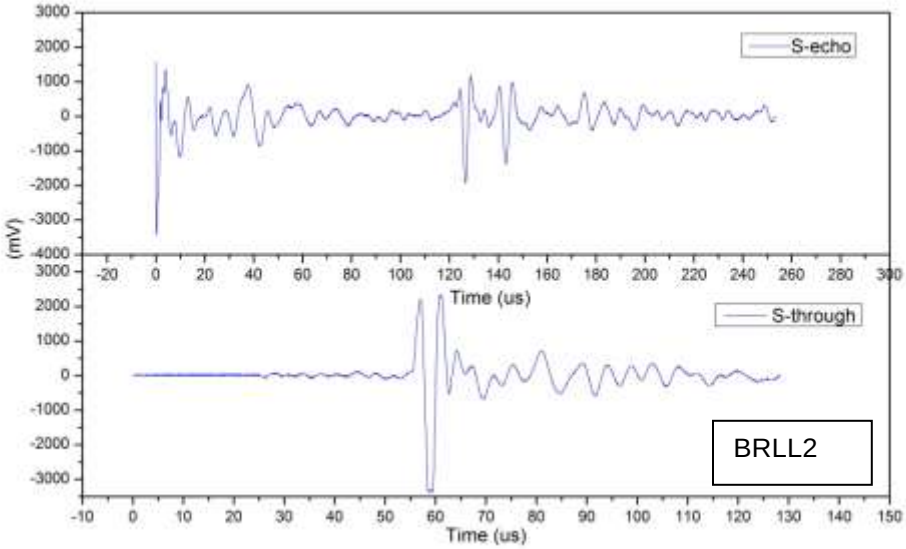


Figure 20. Winchell Limestone S-wave signal. S echo is the signal recorded from one transducer as the wave propagates through the sample and back to the transducer. S echo is not used in this study.

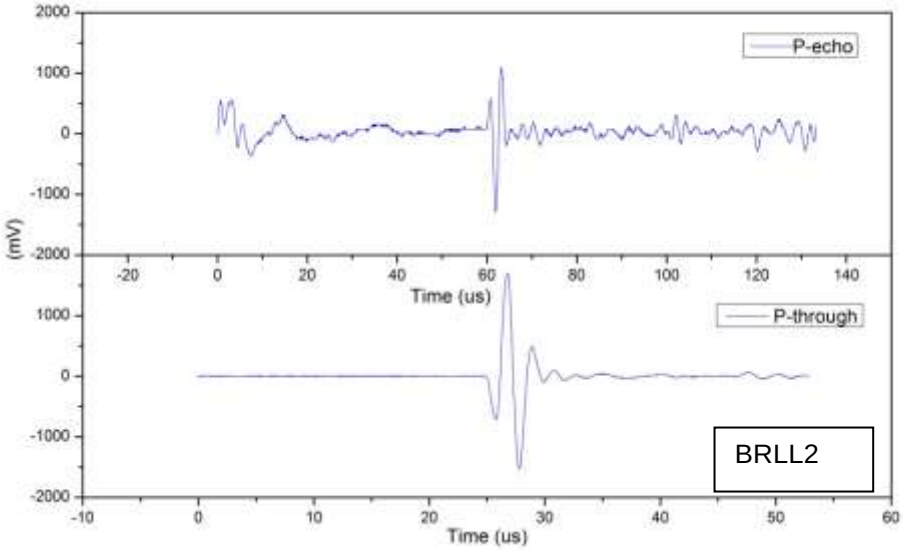


Figure 21. Winchell Limestone P-wave signal. P echo is the signal recorded from one transducer as the wave propagates through the sample and back to the transducer. P echo is not used in this study.

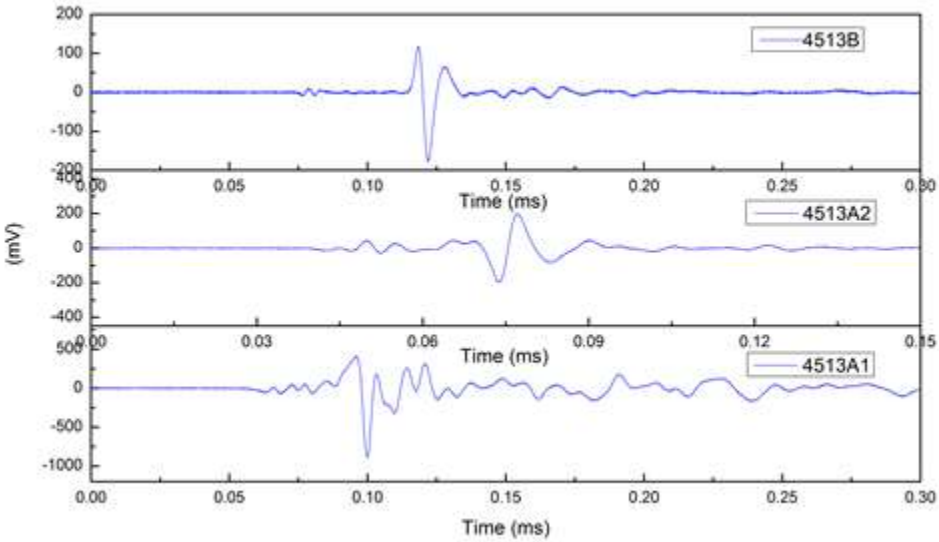


Figure 22. Whitehorse Group S-wave signal.

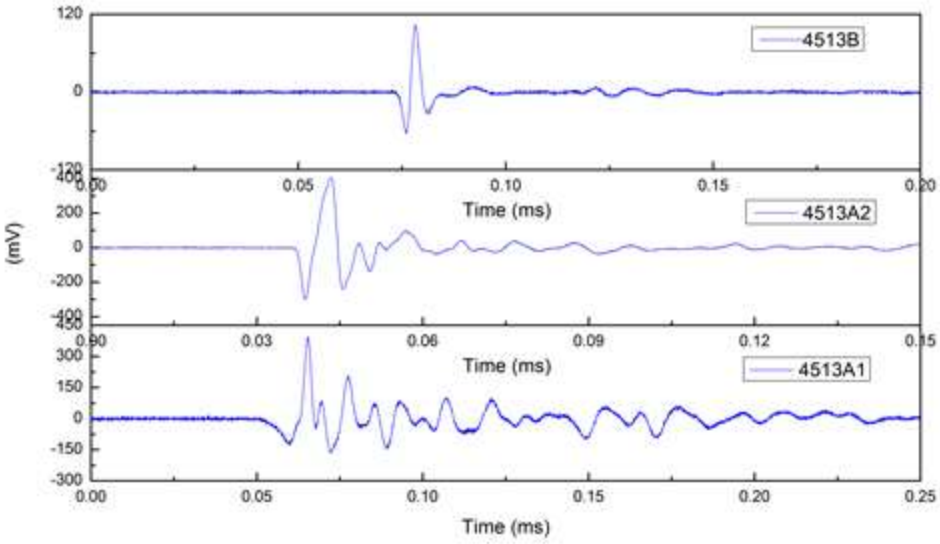


Figure 23. Whitehorse Group P-wave signal.

Looking at the P and S wave acoustic signal, it can be seen that the wave propagation of SALLS (Figure 18 and 19) has been affected by the presence of fractures parallel to the longitudal axis. This causes internal reflection within the sample resulting in interference within the received signal. It was determined that the initial retrieval time of the acoustic wave is accurate and interference occurred in the signal retrieved later on. When observing the S wave signal of SAUS (Figure 18), the peak to peak measurement is taken from the second peak set. This is because the first peak set received by the transducer is the P wave signal, which travels faster through the rock than the desired S wave.

Table 4. P and S wave velocity measurements.

| rock sample | length (mm) | travel time (us) | | Wave velocity (m/s) | |
|---|---|---|---|---|---|
| | | p-wave | s-wave | p-wave | s-wave |
| SAUS | 204.55 | 95.17 | 143.9 | 2149.3 | 1421.5 |
| SALLS | 228.13 | 78.71 | 128.3 | 2898.4 | 1778.1 |
| BCS2 | 157.33 | 23.82 | 40.44 | 6605.0 | 3890.5 |
| BRLL2 | 218.91 | 26.77 | 57.03 | 8177.44 | 3838.51 |
| 4513B | 181.36 | 78.3 | 118.4 | 2316.22 | 1531.76 |
| 4513A2 | 143.30 | 43.3 | 77.3 | 3309.47 | 1853.82 |
| 4513A1 | 173.96 | 62.5 | 95.9 | 2783.36 | 1813.97 |

Supplemental values for fracture density, acoustic velocity and density was acquired from Wickham (1985) to support the data measured in the project. To measure acoustic velocity Wickham (1985) used a method designed by Dr. Mike Batzle, now at the Colorado School of Mines. Samples had their ends machined flat to a tolerance of 0.001” and then measured with a micrometer. In order to measure velocities under both wet and dry conditions the samples were encapsulated in a soft resin. Before the resin was applied to the samples, the samples were wrapped in a wire screen to allow pore water to saturate the specimen. The sample and screen was then wrapped in tape to keep the resin out of the screen.

Acoustic velocities were measured in a triaxial testing machine that could control both confining pressure and pore pressure. The transducers were placed against the samples through holes that were put in the encasing resin and then sealed with a wire clamp to keep the hydraulic oil out of the samples. For each sample three acoustic velocity measurements were measured: a P wave and two S wave velocities 90° apart. The electrical signal from the transducers was amplified and sampled every 50 nano-seconds and displayed on a digital oscilloscope. The transit time through the specimen and the transducers was measured on the oscilloscope to 0.05 micro-seconds.

Measurements of the travel time were made at eight different confining effective pressures; 50, 1000, 2000, 3000, 4000, 6000, and 8000 psi. These eight measurements were first conducted when the specimen was dry, and then repeated after the specimen was saturated with pore water at a pore fluid pressure of 1500 and 3000 psi.

Some problems were encountered in the testing procedure. The most prevalent problem was that many samples did not get pore fluid flow established through the specimen. As a result it was uncertain whether they were saturated and therefore the magnitude of the pore pressure was not reliable. For those specimens the saturated velocity was not taken.

For consistency in the evaluated data sets, and the assumption of dry surface conditions when fractures formed, the unsaturated acoustic velocity data from Wickham (1985) at 50 psi was used. This data is the closest available data set to the laboratory measurement conducted by the Geomechanics Lab at UTA.

Table 5. Velocity data from Wickham (1985).

| Sample Number | $V_p$ (m/s) | $V_s$ (ave) (m/s) |
|---|---|---|
| Brushy Canyon Formation | | |
| 85101711 | 4161.74 | 2607.26 |
| 85101721 | 4112.97 | 2767.28 |
| 85101731 | 4445.2 | 2881.27 |
| Winchell Formation | | |
| 8582713 | 6013.09 | 3140.2 |
| 8582712 | 6101.18 | 3234.54 |
| 8582611 | 6316.37 | 3351.89 |
| 8582714 | 6201.16 | 3294.43 |
| 8582615 | 6338.01 | 3361.33 |
| 8582614 | 6271.56 | 3351.28 |
| Whitehorse Group | | |
| 8510141 | 4521.1 | 2638.81 |
| s8510142 | 3128.77 | 2118.82 |
| 8510143 | 4237.63 | 2547.52 |
| 85101522 | 2261.01 | 1452.98 |
| 85101521 | 3049.83 | 1720.6 |

### 3.2.2 Density Measurement

Samples were cut to a size that available lab equipment could accurately measure (Figure 24). Dry weight was measured for each sample using a digital scale after the sample was allowed to dry over a period of two weeks to allow fluids present within the pore space to evaporate. Following the dry weight measurements, a volume test was conducted by placing the dry samples into a graduated cylinder and

recording the observed displacement of the water. To account for pore space that might be present within the rock specimen the samples were saturated in water for a period of 24 hours (Figure 25). After this period of time it was determined that the available pore space had been filled.

The samples then had their saturated weights recorded immediately after being removed from the water. The amount of water that is present within the pore space when weighed is represented by the difference between the saturated weight and the dry weight of the sample. The porosity of the sample was found using:

$$Por.\% = \left(\frac{W_s - W_d}{V}\right) 100 \qquad \text{(Eq. 22)}$$

After the dry and saturated weight, volume displacement, and porosity were recorded, the dry and saturated density for the samples was calculated. To calculate dry density, the weight of the dry sample was divided by the total volume displacement. This project makes the assumption of dry surface conditions, the unsaturated density of the samples is used in the calculation of Eq. 7b and 7a. The same procedure was conducted with the saturated weight values to calculate the saturated density.

There are some sources of error in the density calculation. One of the errors is the loss of mass in poorly lithified sandstones when the samples are saturated. Sample SAUS lost approximately 1 gram of mass by disaggregating in the water during the 24 hour saturation period. To retrieve the disaggregated sand, the water had to be evaporated and then the remaining sand collected. Another issue that affects the final density calculation is the graduated cylinder used in the measurement of volume displacement. The available equipment's smallest marked units of measurement were 10mL increments so value for the volume of the sample was estimated to about +/- 2 ml.

Figure 24 Cut samples for density measurements**.**

Figure 25. Samples saturating in water.

Table 6. Density and porosity measurements of collected samples and from Wickham (1985).

| Rock Density Measurement | | | | | | | | |
|---|---|---|---|---|---|---|---|---|
| Sample # | Rock Type | Dry Weight (g) | Saturated Weight (g) | Fluid Density | Volume (ml) | Pore Space % | Dry Density | Saturated Density |
| Whitehorse Group | | | | | | | | |
| 4513A1 | Calcite cemented sandstone | 135.9 | 142.87 | 1.000 | 58 | 12.017% | 2.343 | 0.049 |
| 4513A2 | Calcite cemented sandstone | 132.85 | 138.36 | 1.000 | 50 | 11.020% | 2.657 | 0.689 |
| 4513B | Sandstone | 221.35 | 242.53 | 1.000 | 120 | 17.650% | 1.845 | 1.329 |
| SAUS | Sandstone | 69.652 | 76.795 | 1.000 | 39.000 | 18.317% | 1.786 | 1.969 |
| SALLS | dolomite | 225.840 | 234.880 | 1.000 | 90.000 | 10.044% | 2.509 | 2.609 |
| 8510141 | Limestone | 322.300 | 339.270 | 1.000 | 137.580 | 12.335% | 2.343 | 2.466 |
| 8510142 | Limestone | 218.940 | 230.070 | 1.000 | 92.750 | 12.000% | 2.361 | 2.481 |
| 8510151 | Sandstone | 134.780 | 160.750 | 1.000 | 73.250 | 35.454% | 1.840 | 2.194 |
| 8510143 | Limestone | 303.450 | 316.610 | 1.000 | 125.920 | 10.451% | 2.410 | 2.514 |
| 85101521 | Dolomite | 127.330 | 142.490 | 1.000 | 65.180 | 23.259% | 1.954 | 2.186 |
| 85101522 | Dolomite | 108.660 | 119.590 | 1.000 | 52.040 | 21.003% | 2.088 | 2.298 |
| Brushy Canyon Formation | | | | | | | | |
| BCS2 | Sandstone | 215.400 | 218.000 | 1.000 | 90.000 | 2.889% | 2.393 | 2.422 |
| 85101731 | Sandstone | 258.720 | 260.280 | 1.000 | 102.340 | 1.524% | 2.528 | 2.543 |
| 85101721 | Sandstone | 254.240 | 255.430 | 1.000 | 100.460 | 1.185% | 2.531 | 2.543 |
| 85101711 | Sandstone | 218.590 | 230.420 | 1.000 | 95.440 | 12.395% | 2.290 | 2.414 |
| Winchell Formation | | | | | | | | |
| BRLL2 | Limestone | 290.310 | 290.310 | 1.000 | 104.000 | 0.000% | 2.791 | 2.791 |
| 8582611 | Limestone | 332.960 | 333.600 | 1.000 | 118.790 | 0.539% | 2.803 | 2.808 |
| 8582712 | Limestone | 346.540 | 347.820 | 1.000 | 129.850 | 0.986% | 2.669 | 2.679 |
| 8587513 | Limestone | 208.880 | 212.660 | 1.000 | 80.620 | 4.689% | 2.591 | 2.638 |
| 8582615 | Limestone | 235.740 | 236.080 | 1.000 | 102.340 | 0.332% | 2.303 | 2.543 |
| 8582614 | Limestone | 272.360 | 273.190 | 1.000 | 97.360 | 0.853% | 2.797 | 2.806 |

CHAPTER 4

RESULTS

The goal for this project is to estimate fracture density of a rock unit without having to measure the density directly using Eq. 7a. For the calculations below, the fracture density is known previously and the only assumptions to be made are the values of A and B, as stated previously, are constants related to the strain state of the formation. The results for this project were calculated using Eq. 21 which is Eq. 7a in terms of $V_s$ and $V_p$ along with the predicted values of $K_{IC.}$ To be valid the results of Eq. 7a, 7b, 20 and 21 should plot in a straight line. To calculate if fracture density can be related to strain state, Eq. 21 is used, the results of which can be plotted on a graph to show a linear relationship.

The calculated results are formatted in a way where the relationship between fracture density and strain state will have a linear result when observing a particular unit, where A is the slope of the line present and B is the y intercept respectively. The data from the same and nearby outcrops were grouped together in order to satisfy the constraints of the assumption of constant strain being applied. If valid this should result in Eq. 7b and 20 plotting in a straight line. The results of each test can be seen in the following graphs.

## 4.1 Calculated results of Eq. 7b and 20

### 4.1.1 Brushy Canyon

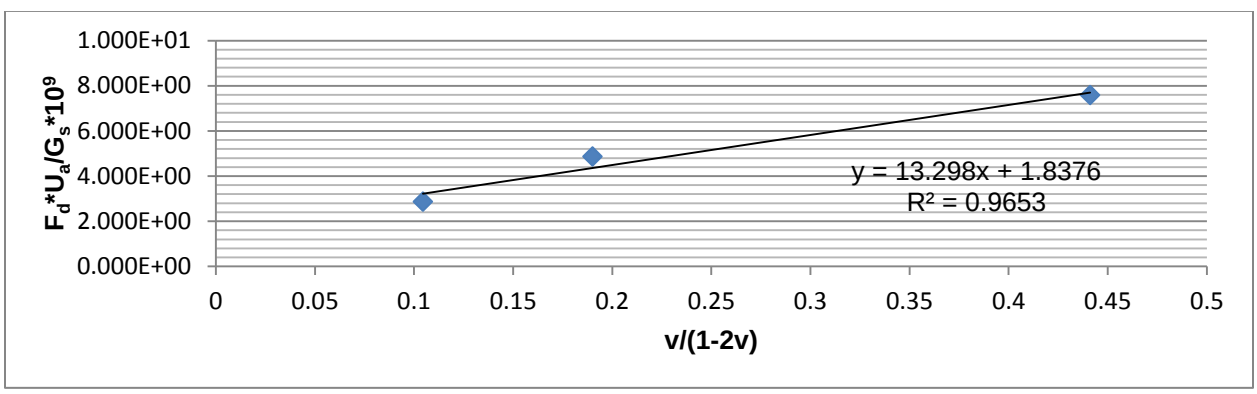


Figure 26. Brushy Canyon test of Eq. 7b and 20.

The Brushy Canyon formation had a correlation coefficient at 0.9653 but due to only three data points the high correlation may not be significant . The linear trend line represented within the graph gives

the values of A and B representing for the first and second strain invariant for the formation. For the Brushy Canyon formation the A is shown to be 13.298 and B is shown to be 1.8376.

4.1.2 Whitehorse Group

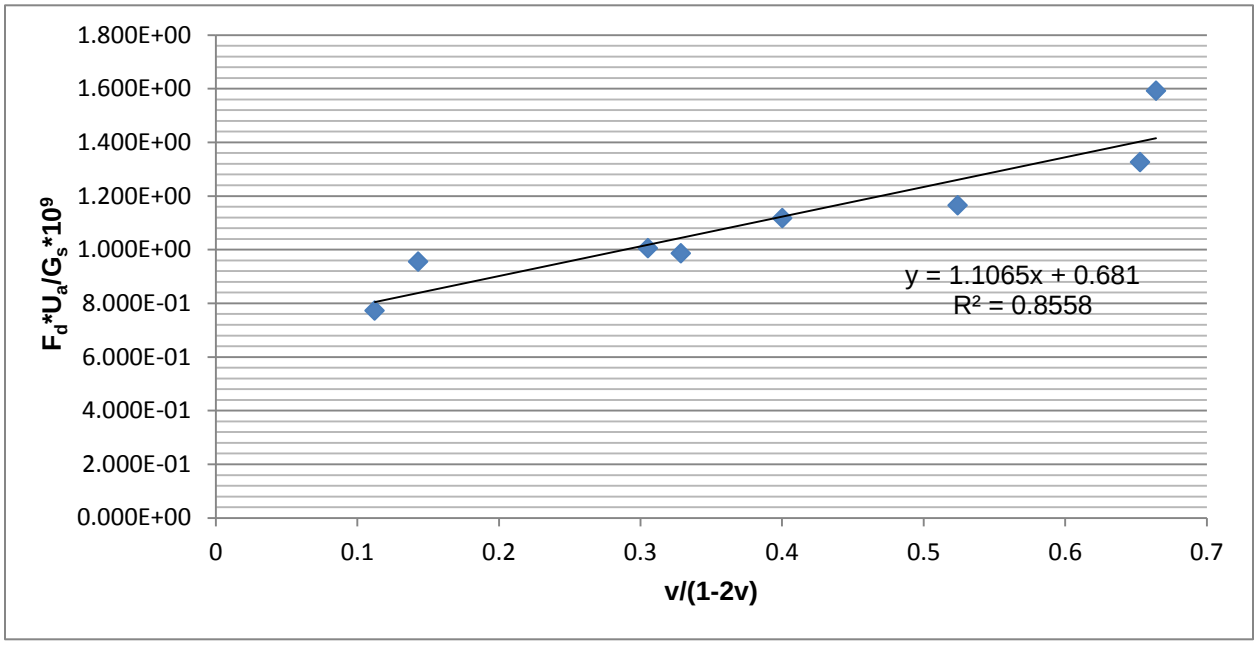


Figure 27. Whitehorse Group calculated test of Eq. 7b and 20.

The Whitehorse Group is shown to have a correlation coefficient of 0.8558. The slope of the linear trend line gives a value of A of 1.1065 and a b value of 0.681. The data set is broad enough to allow for the Wickham (1985) and the 2013 data to plotted separately. When the data set from Wickham 1985 and the 2013 data are graphed individually as in figures 28 and 29 and greater correlation can be seen. The Wickham (1985) (Figure28) data is shown to have a correlation coefficient of 0.9787, an A value of 0.9835 and a B value. The 2013 data (Figure 29) is shown to have a correlation coefficient of 0.9031 with an A value of 1.2907 and a B value of 0.688.

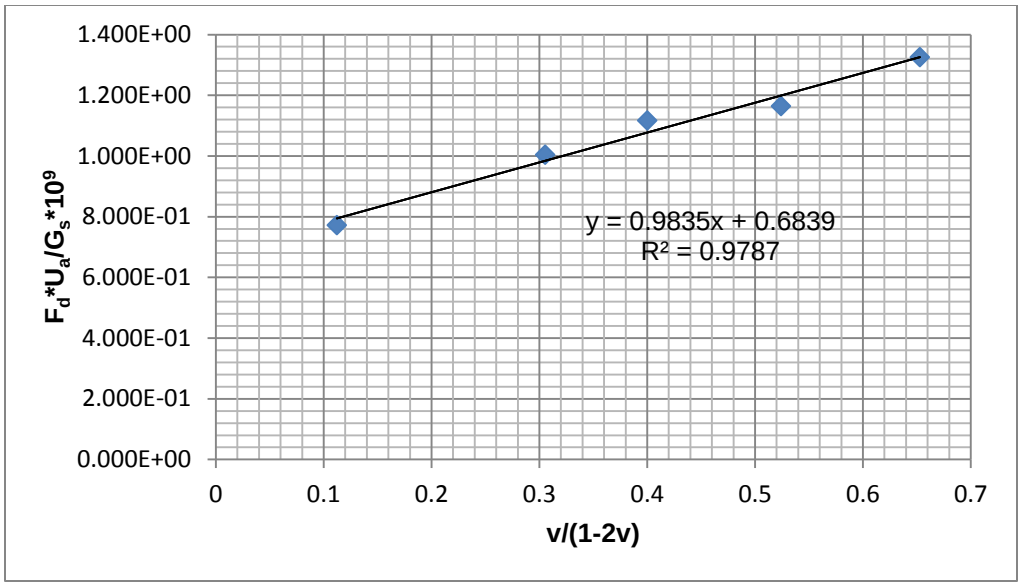


Figure 28. Wickham (1985) Whitehorse Group calculated test of Eq. 7b and 20.

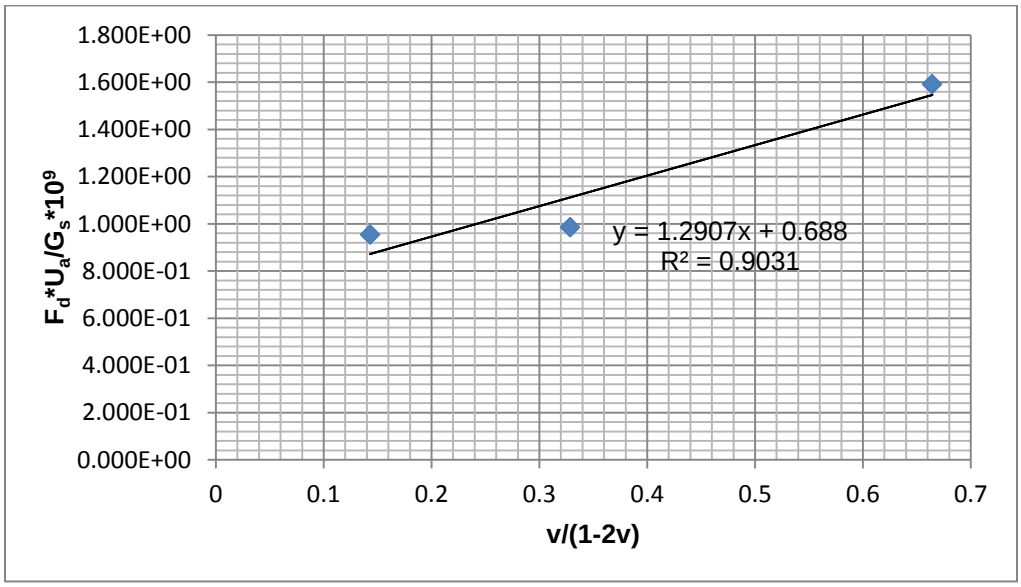


Figure 29. 2013 Whitehorse Group calculated test of Eq. 7b and 20.

4.1.3 Winchell Limestone

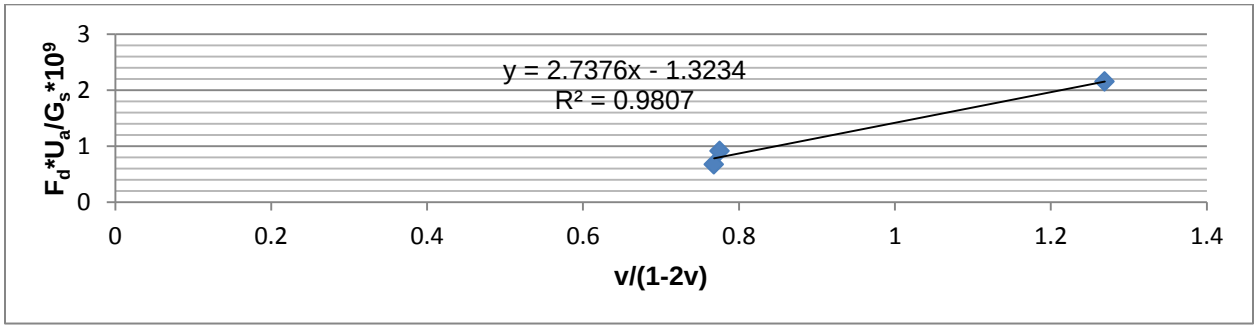


Figure 30. Winchell Limestone calculated test of Eq. 7b and 20.

The Winchell Formation is shown to have a correlation coefficient of 0.9807 but the clustering of the data points indicates that the correlation coefficient is not significant. The slope of the linear trend line gives a value of A of 2.7376 and a B value of as -1.3234. The high correlation illustrated by Figure 30 can be attributed to the Wickham (1985) data points overlapping causing the calculation to act as a correlation between two points instead of three.

## 4.2 Calculated results of Eq. 7a and 21

To calculate $F_d$, the value of A and B derived from the calculation of Eq. 7b and 20 is factored into Eq. 7b and 21 to calculate a predictive value of $F_d$. The predicted value of $F_d$ is plotted against the field measured values of $F_d$ to test the validity of Eq. 7a and 21. Eq. 7a and 21 can be determined as valid if the slope is 1 and the intercept is zero. The correlation coefficient should also be ≥ 0.90.

4.2.1 Brushy Canyon

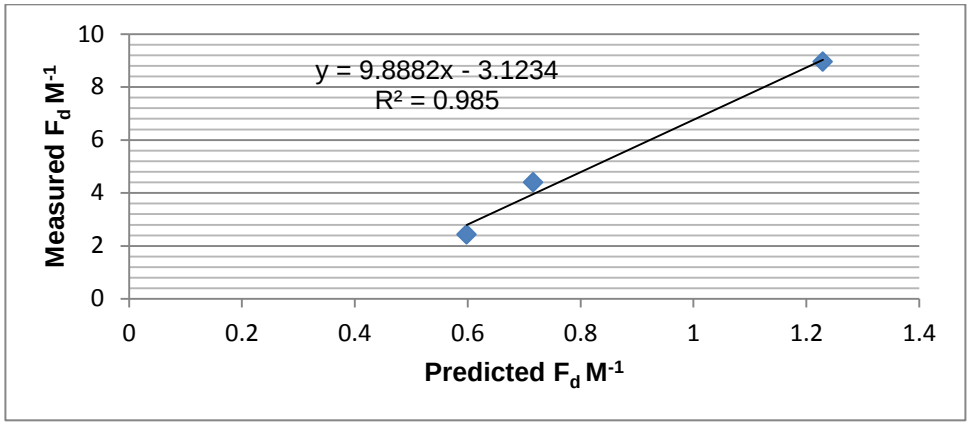


Figure 31. Brushy Canyon calculated test of Eq. 7a and 21.

The values of A and B derived from the Brushy Canyon (Figure 26) are factored into Eq. 7b and 21 to calculate $F_d$. The predicted value of $F_d$ was plotted against the field measured value $F_d$ in figure 21. Although the correlation coefficient is high, the slope and intercept significantly deviate from 1.0 and 0.0 suggesting that some of the assumptions that are made in Eq. 7b do not apply to the Brushy canyon locality.

4.2.2 Whitehorse Group

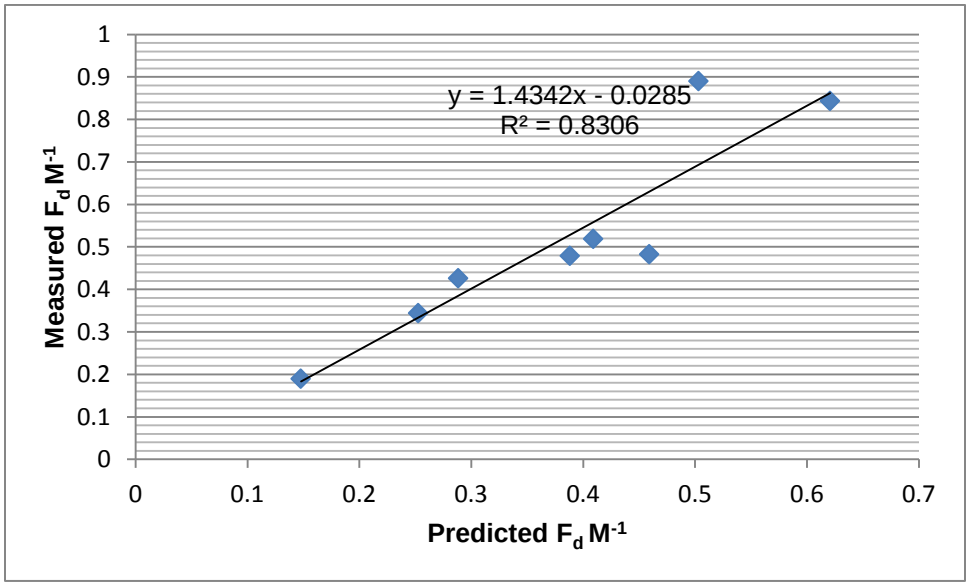


Figure 32. Whitehorse Group calculated test of Eq. 7a and 21 using combined Wickham (1985) and 2013 data.

The plot of the Whitehorse Group has a correlation coefficient of 0.8306 (Figure 32) with a lope and intercept of 1.43 and 0.028 respectively. The data set is large enough to allow for the Wickham (1985) and the 2013 data to plot separately which should increase the correlation coefficient for each data set

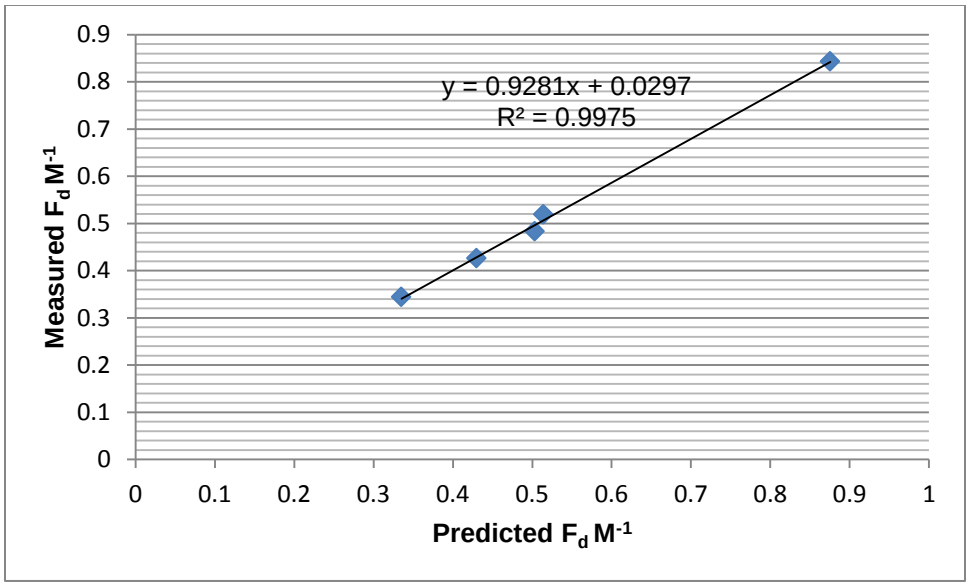


Figure 33. Wickham (1985) Whitehorse Group calculated test of Eq. 7a and 21.

The values of A and B derived from the Whitehorse Group Wickham (1985) (Figure 28) are factored into Eq. 7b and 21 to calculate $F_d$. The predicted value of $F_d$ was plotted against the field measured value $F_d$, giving a correlation coefficient of the trend line of 0.9975 (Figure 33). In addition, the slope is close to 1.0 and the intercept nearly 0.0.

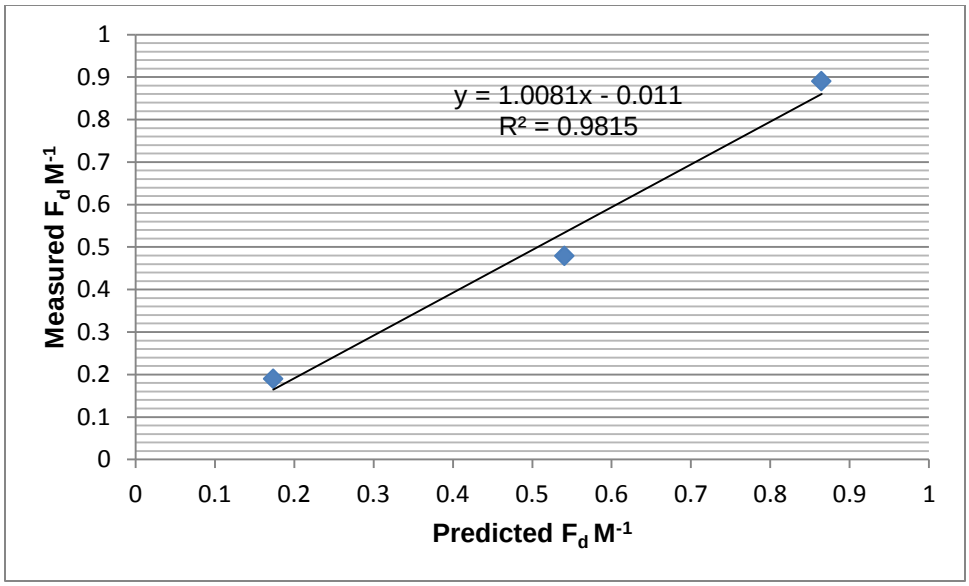


Figure 34. 2013 Whitehorse Group calculated test of Eq. 7a and 21.

The values of A and B derived from the Whitehorse group 2013 data set (Figure 29) are factored into Eq. 7b and 21 to calculate $F_d$. The predicted value of $F_d$ was plotted against the field measured value $F_d$, giving a correlation coefficient of the trend line of 0.9815 (Figure 34). In addition, the slope and the intercept are nearly 1.0 and 0.0 respectively.

4.2.3 Winchell Limestone

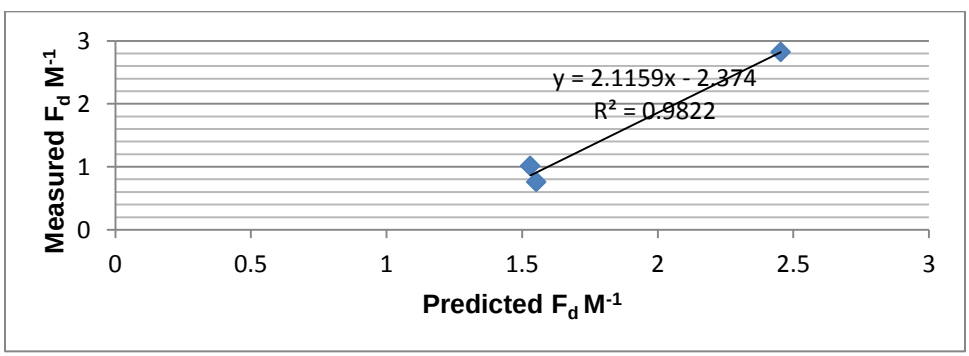


Figure 35. Winchell Limestone calculated text of Eq. 7a and 21.

The values of A and B derived from the Winchell Limestone (Figure 30) are factored into Eq. 7b and 21 to calculate $F_d$. The predicted value of $F_d$ was plotted against the field measured value $F_d$, giving a

correlation coefficient of the trend line of 0.9822 (Fig 35). Due to two of the points clustering, the data set produces a straight line defined by two points resulting in unusable data.

## 4.3 Fracture Density Related to Strain State

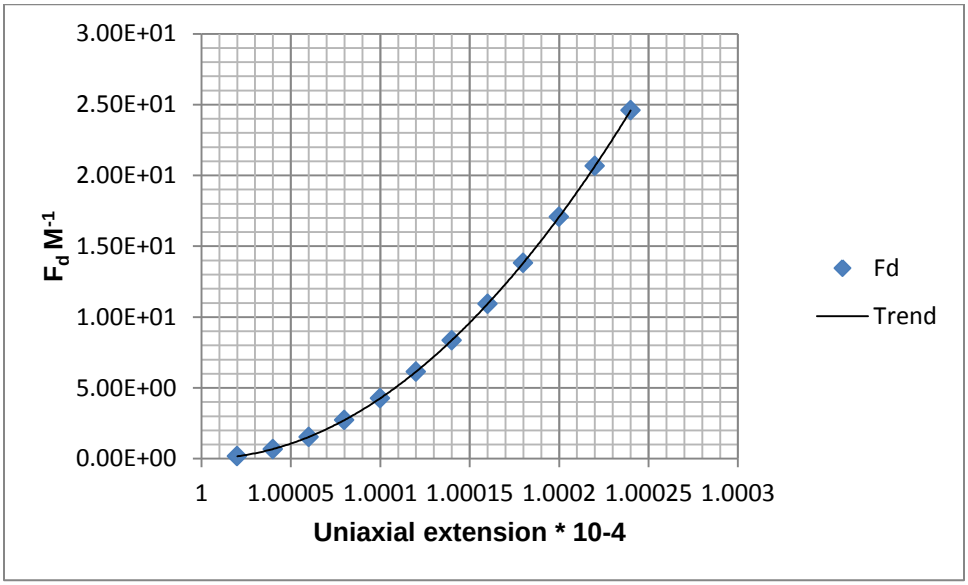


Figure 36. Idealized fracture density development under uniaxial extension, Eq. 7a and Eq. 21

Using equation 7a and 21, the change in $F_d$ and be calculated for a unit as the uniaxial strain that is being applied to the unit changes. The resulting graph will have an exponential increase in $F_d$ as uniaxial extension increases (Figure 36).

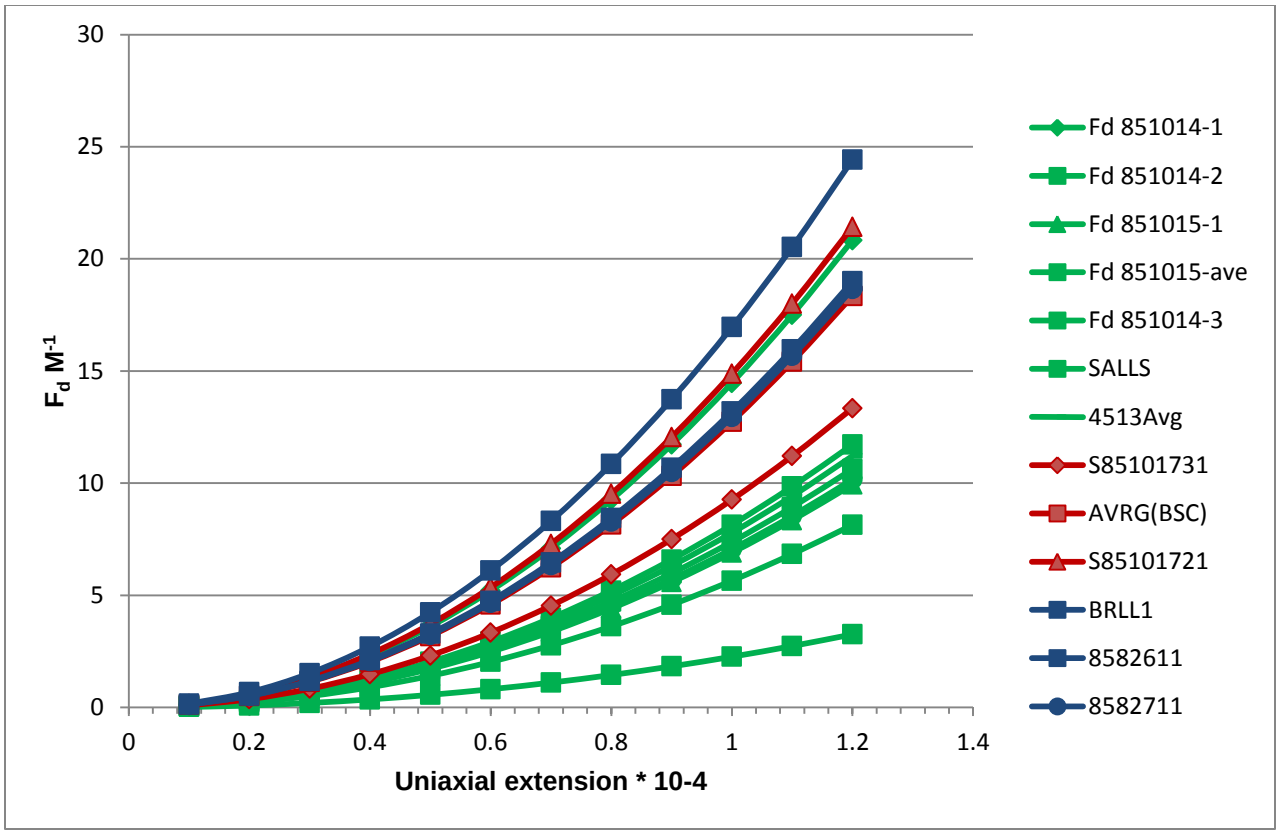


Figure 37. Prediction of fracture density for units in the Whitehorse Group (green), Brushy Canyon (Red) and the Winchell Limestone (Blue), as uniaxial extension increases the strain applied to a formation.

When the physical properties of the different units of the Brushy Canyon, Whitehorse Group and Winchell Limestone are input into Eq. 7a and 21 under increasing uniaxial strain, $F_d$ is shown to have an exponential growth rate (Figure 37). The intensity of in which $F_d$ increases is dependent on the physical rock properties of a unit. The units that were observed to have greater $V_p$ and $V_s$ velocities have a greater $F_d$ value as the uniaxial extension being applied to the unit increases.

# CHAPTER 5

# CONCLUSION

The correlation coefficient of the linear trend line generated from the calculation of Eq. 7b, 20, 7a and 21 had to be ≥ 0.90 for equations 7a and 21 to determined valid, allowing for the prediction of fracture density within geologic units..

Table 7. Calculated results for Eq. 7b, 20, 7a and 21 for the Brushy Canyon, Whitehorse Group and Winchell Formation.

| | Equation | |
|---|---|---|
| Formation | 7b and 20 | 7a and 21 |
| Brushy Canyon | 0.9653 | 0.985 |
| Whitehorse Group Wickham (1985) | 0.9787 | 0.9975 |
| Whitehorse Group 2013 | 0.9031 | 0.9815 |
| Winchell Formation | 0.9807 | 0.9822 |

Due to variation in the method and confining pressure used to acquire acoustic velocity readings from Wickham (1985) and the methods used for this study, the correlation from the combined data sets can result in an artificially low correlation for Eq. 7b and 20 if a larger data set is available, as illustrated within the Whitehorse Group (Figure 27). To correct this problem, the methods used to evaluate $V_p$ and $V_s$ for a data set need to have constant parameters, such as confining pressure. When observed individually, the Whitehorse Group had a correlation of 0.9787 for Wickham (1985) and a correlation of 0.9031 for the 2013 data (Figure 28 and 29) (Table 6). The Brushy Canyon formation data set was not broad enough to allow for the Wickham (1985) and the 2013 data to be evaluated individually and had a resulting correlation of 0.9626 (Figure 26) (Table 6). The Winchell formation could not be separated into different data sets as well and had a correlation of 0.9807 (Figure 30) (Table 6). Both the Brushy Canyon and the Winchell formation did not have enough data points to provide meaningful conclusions.

To calculate Eq. 7b and 21, the value of A and B derived from the calculation of Eq. 7b and 20 (Figure 27-30) is used to provide a predictive value of $F_d$ for the Brushy Canyon, Whitehorse Group and Winchell Formation (Figure 31-35). The correlation for the Brushy Canyon formation was calculated to be 0.9836 (Figure 31) (Table 6). However, the slope and intercept values were significantly different from 1.0 and 0.0 respectively, and there were not enough data points to test the equations. The Wickham (1985)

Whitehorse Group correlation was calculated to be 0.9975 (Figure 33) (Table 6). The 2013 measurements for the Whitehorse Group had a calculated correlation of 0.9815 (Figure 34) (Table 6) and the slope and intercept values are close to 1.0 and 0.0 respectively, suggesting the equations work for this locality. The Winchell formation has a calculated correlation of 0.9822 bit there were not enough data points to make a firm conclusion. The data from the Whitehorse Group are significant, showing both a high correlation coefficient and a slope and intercept near 1.0 and 0.0 on the predicted and observed fracture density graph. There are considerations to be made with the interpretation of the results of this study. The field measurements of fracture density were at the macro scale giving a representative fracture minimum for each geologic unit. Measuring fracture density at the micro scale in addition to the macro scale could result in a higher measured value of $F_d$. Assumption of dry conditions near the surface was made in how the observed joints formed; this assumption could be incorrect while the joints may have formed with pore water under higher pressure.

## 5.1 Application to industry

Hydraulic fracturing is one of the leading methods used in the oil and gas industry today. This term is used to describe the variety of methods that are used in the stimulation of reservoirs. Hydraulic fracturing is conducted after a well bore is completed and wireline logging tools are used to evaluate reservoir conditions. The way a reservoir is stimulated is by the injection of a fracturing fluid through a well bore and against the face of a formation at a pressure that is sufficient to overcome the overburden pressure and to initiate or extend the length of preexisting fractures (Norman et al., 1996). Having knowledge of the natural fracture density of a unit is very important in the planning of fracturing operations. Natural fractures can be used to enhance the recovery of a reservoir beyond what normally would be obtainable in a non-fractured unit. However, natural fractures can be extended beyond the desired unit causing leakage of gas if the pressure of the fracture fluid being injected into the reservoir is too high. For this reason it is important to have the ability to estimate the density of preexisting natural fractures that are present within the unit prior to hydraulic stimulation. Figure 26 through 35 indicate, through the application of Eq. 7a and 21, traditional wireline logs can be used to make a reasonable and accurate estimation of the preexisting fracture density of a unit. Additionally, some geologic units are

more susceptible to hydraulic fracturing than others as function of that unit's brittleness. Equation 7a and 21 can be applied as a measure of a unit's brittleness prior to hydraulic fracturing.

REFERENCES


Adams, J. E., H. N. Frenzel, M. L. Rhode, and D. P. Johnson, 1951, Starved Pennsylvanian Midland basin: AAPG Bulletin 35: 2600–2607.

Anderson, T. L., 1991. Fracture Mechanics, CRC Press, Boca Raton, 793pp.

ASTM (2000). "Standard Test Method for Laboratory Determination of Pulse Velocities and UltrasonicElastic Constants of Rock." ASTM, West Conshohocken, PA, 7.

Atkinson, Barry Kean. 1987. Fracture Mechanics of Rock. Academic Press Geology Series

Backers T. 2005. Fracture toughness determination and micromechanics of rock under mode I and mode II loading. PhD thesis, University of Potsdam

Ball, Mahlon M. 1995 Permian Basin Province, United States Department of the interior, USGS

Barthelemy, J-F, MLE Guiton and J-M Daniel. 2009. Estimates of Fracture Density and Uncertainties from Well Data. International Journal of Rock Mechanics and Mining Sciences 46, (3): 590-603

Barton, C.C. 1995. Fractal Analysis of Scaling and Spatial Clustering of Fractures. In C.C. Barton and P.R. LaPointe, eds., Fractals in the Earth Sciences: New York, Plenum Press: 141-178.

Bourne, S.J., and E.J. Willemse. 2001. Elastic Stress Control on the Pattern of Tensile Fracturing around a Small Fault Network at Nash Point, United Kingdom. Journal of Structural Geology 23: 1753-1770

Busetti, S., K. Mish, Z. Reches, 2012. Damage and plastic deformation of reservoir rocks: Part 1. Damage Fracturing. AAPG Bulletin 96 (9): 1687-1709.

Busetti, S., K. Mish, P. Hennings, Z. Reches, 2012. Damage and plastic deformation of reservoir rocks: Part 2. Propagation of a hydraulic fracture. AAPG Bulletin 96 (9): 1711-1732.

Chiles, J.P., H. Beucher, H. Wackernagel, C. Lantuejoul, P. Elion. 2008. Estimating fracture density from a linear or aerial survey. Proceedings of the VIII International Geostatistics Congress, *ed.* J. Ortiz and X. Emery. V. 1, p. 535-544. http://downloads.gecamin.cl/cierreeventos/geostats2008/prsntcns/00158 00721 p r.pdf.

Corbett, K., M. Friedman and J. Spang. 1987. Fracture Development and Mechanical Stratigraphy of Austin Chalk, Texas. AAPG Bulletin 71 (1): 17-28

Dershowitz, W.S. and H.H. Herda. 1992. Interpretation of Fracture Spacing and Intensity. In J.R. Tillerson and W.R. Wawersik, eds., Proceedings of the 33rd U.S. Symposium on Rock Mechanics. Rotterdam, Balkema: 19-30

Di Naccio, D., P. Boncio, S. Cirilli, F. Casaglia, E. Morettini, G. Lavecchia and F. Brozzetti. 2005. Role of Mechanical Stratigraphy on Fracture Development in Carbonate Reservoirs; Insights from Outcropping Shallow Water carbonates in the Umbria-Marche Apennines, Italy. Journal of Volcanology and Geothermal Research 148, (1-2): 98-115.

Dutton, S. P., E. M. Kim, R. F. Broadhead, W. D. Raatz, C. L. Breton, S. C. Ruppel, and C. Kerans, 2005, Play analysis and leading-edge oil-reservoir development methods in the Permian basin: Increased recovery through advanced technologies: AAPG Bulletin 89: 553–576, doi:10.1306/12070404093.

Ehlen J. 2000. Fractal Analysis of Joint Patterns in Granite. International Journal of Rock Mechanics and Mining Sciences 37: 909-922.

Gillespie, P.A., G.B. Howard, J.J. Walsh, and J. Watterson. 1993. Measurement and Characterization of Spatial Distributions of Fractures. Tectonophysics 226: 113-141

Griffith, A. A. 1921. The Phenomena of rupture and flow in solids. Philosophical Transactions of the Royal Society A221: 163-198.

Grover, George, 1984, Lower Permian to Upper Pliocene carbonate and Clastic Faces, Southwestern Eastern Shelf West Central Texas. Field Trip Guidebook, Permian Basin Section, Society of Economic paleontologist and Mineralogists. (2): 24

Harms, John C., Williamson, Charles R. 1998. Deep-Water Density Current Deposits of Delaware Mountain Group (PERMIAN), Delaware Basin, Texas and New Mexico. AAPG Bulletin 72, (3): 299-317

Huang, Jian-an and Wang, Sijing. 1985. An experimental Investigation Concerning the Comprehensive Fracture Toughness of Some Brittle Rocks. Int. J. Rock Mech, Ming, schi and Beomech. Abstr Vol. 22 (2): 99-104

Hennings, P.H., J.E. Olson and L.B. Thompson. 2000. Combining Outfrop Data and three-dimensional Models to Characterize Fractured Reservoirs: An Example from Wyoming. AAPG Bulletin 84, (6): 830-849

Hills, J. M., 1970, Late Paleozoic structural directions in southern Permian basin, west Texas and southern New Mexico: AAPG Bulletin 54: 1809–1827

Hills, J. M., 1984, Sedimentation, tectonism, and hydrocarbon generation in Delaware basin, west Texas and southeastern New Mexico: AAPG Bulletin 68: 250–267.

Hills, J. M., and J. E. Galley, 1988, The Permian basin region, in the geology of North America, sedimentary cover—North American craton: Geological Society of America, v. D-2, 261–276.

Huang, Q., and J. Angelier. 1989. Fracture Spacing and its Relation to Bed Thinkness. Geological Magazine 126: 355-362

Irwin, G. R., 1956. Onset of Fast Crack Propagation in High Strength Steel and Aluminum Alloys, Sagamore Research Conference Proceedings, Vol. 2, 289-305.

Julander, D.R., P.F. Cowell, H. Wu, and J.A. Angehrn. 1999. An Investigation of Subsurface Fracture Distribution in the Monterey Formation, Lost Hills Oil Field, CA using Borehole Image Logs and Whole Core. AAPG Bulletin 83, (4): 692-692

Karaman, A., and P.J. Carpenter. 1997. Fracture Density Estimates in Glaciogenic Deposits from P-wave Velocity Reductions. Geophysics 62, (1): 138-148.

Ladeira, F.L. and N.J. Price. 1981. Relationship between Fracture Spacing and Bed Thickness. Journal of Structural Geology 3: 179-183

LaPointe, P.R. 1988. A Method to Characterize Fracture Density and Connectivity through Fractal Geometry. International Journal of Rock Mechanics and Mining Sciences & Geomechanics Abstracts 25 (6): 421-429

LaPointe, P.R. 2002. Derivation of Parent Fracture Population Statistics from Trace Length Measurements of Fractal Fracture Populations. lnternation Journal of Rock Mechanics and Mining Sciences 39: 381-388.

LaPointe, P.R. and J.A. Hudson. 1985. Characterization and Interpretation of Rock Mass Joint Pattern. Geological Society of America Special Paper 199: 1-37.

Lezin, C., F. Odonne, G.J. Massonnat and G. Escadeillas. 2009. Dependence of Joint Spacing on Rock Properties in Carbonate Strata. AAPG Bulletin 93 (2): 271-290

Lindsay, R. F., 2009. West Texas Structure. Center for Energy and Economic Diversification, University of Texas of the Permian Basin. http://ceed.utpb.edu/geology-resources/west-texas-geology/west-texas-structure/

Lorenz, J.C., S.P. Cooper, and W.A. Olsson, 2006. Natural Fracture Distributions in Sinuous, Channel-fill Sandstones of the Cedar Mountain Formation, Utah. AAPG Bulletin 90, (9): 1293-1308

Luo, M., 1992, Generation and development of the overpressure system in the eastern Delaware basin, west Texas and southern New Mexico: Ph.D. dissertation, University of Texas at El Paso, El Paso, Texas, 190 p.

Lou, M., and J.A. Rial. 1997. Characterization of Geothermal Reservoir Crack Patterns using Shear-Wave Splitting. Geophysics 62 (2): 487-494

Maley, V. C., and R. M. Huffington, 1953, Cenozoic fill and evaporate solution in the Delaware basin, Texas and New Mexic.: AAPG Bulletin 64: 539–546.

Martin, Robert H., Christensen, M. H., Gross, R. E., Vaughn, W. J. 1954. Developments in West Texas and Southeastern New Mexico in 1953. AAPG Bulletin 38 (6): 1139-1155

Mauldon, M., W.M. Dunne and M.B. Rohrbaugh. 2001. Circular Scanlines and Circular Windows; New Tools for Characterizing the Geometry of Fracture Traces. Journal of Structural Geology 23, (2-3): 247-258

Maultzsch, S., M. Chapman, E. Liu, X-Y. Li. 2003. Modeling Frequency Dependent Seismic Anisotropy in Fluid Saturated Rocks with aligned Fractures; Implication of Fracture Size Estimation from anisotropic Measurements. Geophysical Prospecting 51 (5): 381-392

Maxwell, S.C. and T.l. Urbancic. 2005. The Potential Role of Passive Seismic Monitoring for Real-Time 40 Reservoir Characterization. SPE Reservoir Evaluation and Engineering 8 (1): 70-76.

McCann, D. M. and Entwisle D. C. 1992. Determiniation of Young's modulus of the Rock Mass From Geophysical Well Logs. Geological Application of Wireline Logs II. Geological Society Special Publication 65: 317-225

Mclennan, J.A., P.F. Allwardt, P.H. Hennings, and H.E. Farrell. 2009. Multivariate Fracture Intensity Prediction; Application to Oil Mountain Anticline, Wyoming. AAPG Bulletin 93, (11): 1585-1595.

McQuillan, H. 1974. Fracture Patterns on Kuh-e Asmari Anticline, Southwest Iran. AAPG Bulletin 58 (2): 236-246

Montgomery, Scott L, Worrall, John, Hamiltion, Dean. 1999 Delaware Mountain Group, West Texas and Southern New Mexico, A case of Refound Opportunity; Part 1 – Brushy Canyon. AAPG Bulletin 83, (12):1901-1926

Murray, G.H. 1968. Quantitative Fracture Study: Sanish Pool, McKenzie County, North Dakota. AAPG Bulletin 52, (1): 57-65.

Myers, Donald A. 1955. Stratigraphic Distribution of Some Pennsylvanian from Brown and Coleman Counties, Texas. United States Department of the Interior, Geological Survey Professional Papers 315: 37-53

Narr, W. and I. Lerche. 1984. A Method for Estimating Subsurface Fracture Density in Core. AAPG Bulletin 68, (5): 637-648

Narr, W. and J. Suppe. 1991. Joint Spacing in Sedimentary Rocks. Journal of Structural Geology 13: 1037-1048.

Norman, William D., Jasinski, Raymond L., Neison, Erik B. 1996. Hydraulic Fracturing Process and Compositions. Patent US5551516, Sep 3, 1996

Ortega, O.J., R.A. Marratt and S.E. Laubach. 2006. A Scale-Independent Approach to Fracture Intensity and Average Spacing Measurement. AAPG Bulletin 90, (2): 193- 208

Page, Lincoln R. and Adams, John Emery. 1940. Stratigraphy, Eastern Midland Basin, Texas. AAPG Bulletin 24, (1): 52-208

Palchik, V. and Y.H. Hatzor. 2002. Crack Damage Stress as a Composite Function or Porosity and Elastic Matrix Stiffness in Dolomites and Limestones. Engineering Geology 63: 233-245

Peacock, D.C.E., S.D. Harris, and M. Mauldon. 2003. Use of Curved Scanlines and Boreholes to Predict Fracture Frequency. Journal of Structural Geology 25: 109-119.

Pollard, D.O., and P. Segal. 1987. Theoretical Displacements and Stresses near Fractures in Rock: With Applications to Faults, Joints, Veins, Dikes and Solution Surfaces, in B.K. Atkinson, ed., Fracture Mechanics of Rock: New York, Academic Press Geology Series: 277-349.

Priest, S.D. and J.A. Hudson. 1976. Discontinuity Spacings in Rock. International Journal of Rock Mechanics and Mining Sciences and Geomechanical Abstracts 13: 135-148.

Renshaw, C.E. 1997. Mechanical Controls on the Spatial Density of Opening-Mode Fracture Networks. Geology 25: 923-926

Schultz-Eia, D.O. and J. Yeh. 1992. Predicting Fracture Permeability from Bed Curvature. Proceedings of the 33rd U.S. Symposium on Rock Mechanics 33: 579-589

Sheriff, R.E., 1991, Encyclopedic Dictionary of Exploration Geophysics, 3rd ed. Society of Exploration Geophysics, Tulsa, OK

Sih, G. C. 1985. Mechanics and Physics of Energy Density Theory. Theoretical and Applied Fracture Mechanics 4: 157-173

Slatt, Roger M. and Abousleim, Younane, 2011. Merging Sequence Stratigraphy and Geomechanics for Unconventional Gas Shales. The Leading Edge: 274-282

Stearns, D.W. 1967. Certain Aspects of Fracture in naturally Deformed Rocks. In R.E. Riecker, ed. Rock Mechanics Seminar: US Air Force Cambridge Research Laboratories. Contribution AD 669375: 97-118.

Stearns, D.W. and M. Friedman. 1972. Reservoirs in Fractured Rock, in R.E. King, ed., Stratigraphic Oil and Gas Fields: Classification, Exploration Methods, and Case Histories. AAPG Memior 16: 82-106.

Tapp, B., S. McGinty-Davis, L. Lortz and M. Schlagel. 1999. Fracture Architecture of the Tensleep Sandstone, Bighorn Basin, Wyoming; Surface Analogs for Subsurface Reservoirs. AAPG Bulletin 83, (7): 1189-1189.

Veatch, R.W. 1983. Overview of Current Hydraulic Fracturing Design and Treatment Technology- Part I. Journal of Petroleum Technology 35, (4): 677-687

Velde, B.J., J. DuBois, G. Touchard, and A. Badri. 1990. Fractal Analysis of Fractures in Rocks: The Cantor's Dust Method. Tectonophysics 179: 345-352

Watts, N.L., 1983, Microfractures in Chalks of Albuskjell Field, Norwegian Sector, North Sea; Possible Origin and Distribution. AAPG Bulletin 67, (2): 201-234

West Texas Geologic Society, 1960, Geology of the Delaware Basin and field trip guidebook: Sept. 29th, 30th, and Oct. 1st,: 42 – 49

Whittaker, Barry N., Singh, Raghu N., Sun, Gexin. 1992. Rock Fracture Mechanics Principles, Design and Applications. Developments in Geotechnidal Engineering 71: 349-371

Wickham, J. S., G. Tapp and J. Reddy, 1982, Finite-Element Modelling of Fracture Density in Single Layer Folds. International Journal for Numerical & Analytical Methods in Geomechanics 6: 441-459

Wickham, J.S., X. Yu, R. McMullen (2013) Geomechanics of Fracture Density. Unconventional Resources Technology Conference, Paper 1619745 in press

Willemse, E.J.M., D.C.P. Peacock, A. Aydin and D.O. Pollard. 1997. Relationship between Faults and Fractures in Tight Reservoirs. AAPG Bulletin 81: 1419-1420.

Wright, Wayne R., 2011. Pennsylvanian Paleodepositional Evolution of the Greater Permian Basin, Texas and New Mexico: Depositional Systems and Hydrocarbon Reservoir Analysis. AAPG Bulletin 95 (9): 1525-1555

Wu, H. and D.D. Pollard. 1995. An Experimental Study of the Relationship between Joint Spacing and Layer Thickness. Journal of Structural Geology 17: 887-905

Wu, H. and D.O. Pollard. 2002. Imaging Fracture Networks around Boreholes. AAPG Bulletin 86 (4): 593-604.

Xu, X., and I. Tsvankin. 2007. A Case Study of Azmuthal AVO Analysis with Anisotropic Spreading Correction. Leading Edge 26, (12): 1552-1561.

Yang, Kenn-Ming, Dorobek, Steven L. 1995. The Permian Basin of West Texas and New Mexico; Flexural Modeling and evidence for Lithospheric Heterogeneity Across the Marathon Foreland. SEPM Special Publication 52.

Zahm, C. and P.H. Hennings. 2009. Complex Fracture Development Related to Stratigraphic Archetecture; Challenges for Structural Deformation Prediction, Tensleep Sandstone at the Alcove Anticline, Wyoming. AAPG Bulletin 93, (11): 1427-1446

Zhixi, C., Mian, C., Yan, J., Rongzun, H., 1997. Determination of Rock Fracture Toughness and its Relationship with Acoustic Velocity; Int. J. Rock Mech. And Min. Sci. 34: 3-4, Paper No. 49

## BIOGRAPHICAL INFORMATION

Skyler Smith attended Texas Tech University in 2006 for his undergraduate degree. While at Texas Tech, Skyler received a bachelor's degree in Geoscience with a concentration in Geology and a minor in Geographic Information Systems. His interest as an undergraduate was over sedimentology and he conducted research over facies analysis of the Stockweather Limestone in relation to changes in global glaciation levels. In 2011, Skyler attended The University of Texas at Arlington to study Petroleum Geology. His research interest was towards unconventional resources and this led to a focus towards rock mechanics and hydraulic fracturing. After Graduation Skyler intends to working in new ventures hydrocarbon exploration for an oil and gas company before opening his own oil exploration firm.